Dmitrijs Prigunovs

DEVELOPMENT OF AN EFFECTIVE OPTICAL AMPLIFIER AND PERFORMANCE EVALUATION IN COMMUNICATION SYSTEMS

Summary of the Doctoral Thesis

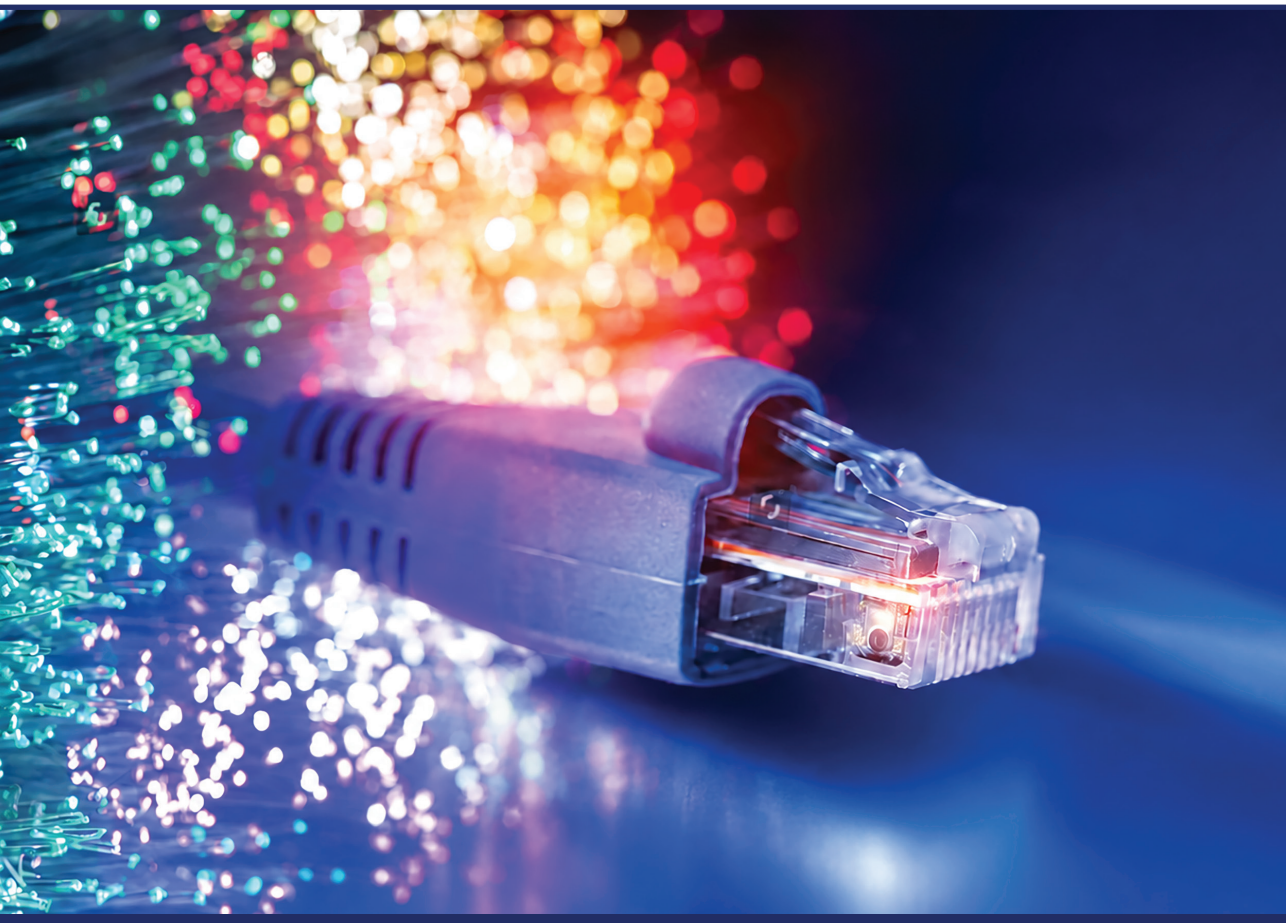

RTU Press
Riga 2026

RIGA TECHNICAL UNIVERSITY
Faculty of Computer Science, Information Technology and Energy
Institute of Photonics, Electronics and Telecommunications

Dmitrijs Prigunovs

Doctoral Student of the Study Programme "Telecommunications"

DEVELOPMENT OF AN EFFECTIVE OPTICAL AMPLIFIER AND PERFORMANCE EVALUATION IN COMMUNICATION SYSTEMS

Summary of the Doctoral Thesis

Scientific supervisors

Professor Dr. sc. ing.
VJAČESLAVS BOBROVS

Associate Professor Dr. sc. ing.
TOMS SALGALS

Riga 2026
RTU Press

Prigunovs, D. Development of an Effective Optical Amplifier and Performance Evaluation in Communication Systems. Summary of the Doctoral Thesis. Riga: RTU Press, 2026. – 53 p.

Published in accordance with the decision of RTU Promotion Council "P-08" of 17 April 2026, Minutes No. 49.

Cover image by Dmitrijs Prigunovs.

https://doi.org/10.7250/9789934373244
ISBN 978-9934-37-324-4 (pdf)

DOCTORAL THESIS PROPOSED TO RIGA TECHNICAL UNIVERSITY FOR PROMOTION TO THE SCIENTIFIC DEGREE OF DOCTOR OF SCIENCE

To be granted the scientific degree of Doctor of Science (PhD), the present Doctoral Thesis has been submitted for defence at the open meeting of the RTU Promotion Council on 28 August 2026, at 11.00 AM at the Faculty of Computer Science, Information Technology and Energy of Riga Technical University, Āzenes iela 12, Room 201.

OFFICIAL REVIEWERS

Dr. sc. ing. Aleksandrs Ipatovs,
Riga Technical University

Dr. sc. ing. Inga Brice,
University of Latvia, Latvia

Dr. sc. ing. Anna Baldycheva,
Exeter University, UK

DECLARATION OF ACADEMIC INTEGRITY

I hereby declare that the Doctoral Thesis submitted for review to Riga Technical University for promotion to the scientific degree of Doctor of Science (PhD) is my own. I confirm that this Doctoral Thesis has not been submitted to any other university for promotion to a scientific degree.

Dmitrijs Prigunovs: _____

Date: _____

The Doctoral Thesis has been developed as a set of thematically related scientific publications with a summary in Latvian and English. It has been written in Latvian and consists of an Introduction, five chapters, Conclusions, 54 figures, 3 tables, and eight appendices; the total number of pages is 93 (not including appendices). The Bibliography contains 104 titles. The PhD Thesis presents a summary of 8 original scientific articles out of 19 articles published by the author and one patent issued by the Republic of Latvia. Scientific publications have been written in English and are indexed in SCOPUS, IEEE and WoS databases; their total volume is 69 pages.

ABSTRACT

The Doctoral Thesis investigates and analyses several scientific studies regarding the use of EDFA, Raman, FOPA, and hybrid optical amplifiers in wavelength-division multiplexed (*WDM*) communication systems. Computer simulation software – specifically RSoft OptSim and VPIphotonics Design Suite – was employed. Particular attention is paid to optical amplifiers utilising dual rare-earth-doped fibers and an in-fiber cladding-pumping technique.

The Thesis also evaluates a method for broadening 50 ps electrical pulses using a high-precision event timer, Bessel and Butterworth filters, and various custom-built cascaded low-pass filters (*LPF*). Bit Error Rate (*BER*) performance was analysed for both optical back-to-back (*B2B*) configurations and configurations involving 20 km transmission over single-mode fiber (SMF), utilising a pulse duration (τ) of 50 ps and varying pulse width values (Δ): 50 ps, 100 ps, and 200 ps.

The fabrication of spherical lenses – or microspheres – was demonstrated using the commercially available Fujikura-100P+ arc fusion splicer, a device employed for integrated photonic devices.

Keywords

Erbium/ytterbium doped fiber amplifier (EYDF), Fiber optical parametric amplifier (FOPA), Pulse position modulation (PPM), lensed fiber

LIST OF ABBREVIATIONS

A

ASE	Amplified Spontaneous Emission
ADC	Analog-To-Digital Converter
AWG	Arrayed Waveguide Grating

B

BER	Bit-Error-Rate

C

CAPEX	Capital Expenditure
CD	Chromatic Dispersion
CWDM	Coarse Wavelength Division Multiplexing

D

DWDM	Dense Wavelength Division Multiplexing
DSO	Digital Storage Oscilloscope
DC	Double-Core

E

EYDFA	Erbium/Ytterbium Doped Fiber Amplifier
EYDF	Erbium/Ytterbium Doped Fiber
EDFA	Erbium Doped Fiber

F

FOPA	Fiber Optical Parametric Amplifier
FWM	Four-Wave Mixing
FP	Filtered Pulse
FWHM	Full Width of Half Maximum
FBG-DCM	Fiber Bragg Grating Dispersion Compensating Module

H

HNLF	High Nonlinear Fiber

G

GP	Generated Pulse

I

IL	Insertion Losses
IR-UWB	Impulse Radio Ultra-Wideband

L

LPF	Low-Pass Filter

M

MC	Multi-Core

O

OPEX	Operating Expense
OOK	On-Off Keying
OBPF	Optical Band Pass Filter
OB2B	Back-To-Back
OF	Optical Filter
OSNR	Optical Signal-to-Noise Ratio
ODN	Optical Distribution Network
ON	Optical Terminal Network

P

PON	Passive Optical Network
PRBS	Pseudorandom Binary Sequence
PPM	Pulse Position Modulation

Q

QPSK	Quadrature Phase-Shift Keying

R

REDFA	Rare Earth Doped Fiber Amplifier
RA-FOPA	Raman-based parametric amplifier on optical fiber

S

SMF	Single Mode Fiber
SMD	Spatial-Division Multiplexing
SNR	Signal To Noise Ratio
SSE	Stimulated Spontaneous Emission
SRS	Stimulated Raman Scattering
SBS	Stimulated Brillouin Scattering
ŠOPS	Fiber Optical Transmission System

T

TDC	Time Digital Converter
TR-PPM	Modulation Of The Transmitted Reference Pulse Position

U

UWB	Ultra-Broadband

Table of Contents

RELEVANCE OF THE TOPIC

The development of modern information and communication technologies is connected with a continuous increase in the volume of transmitted information, which requires an increase in the capacity and transmission distance of optical fiber communication systems. To meet these requirements, wavelength division multiplexing (*WDM*) systems have become widely used, allowing multiple channels to be transmitted simultaneously over a single fiber [1–3]. However, when transmitting signals over long distances, they inevitably weaken in the optical fiber due to material loss, bending, and connections, so the use of optical amplifiers is an integral part of today's main communication lines. The most effective and technologically advanced type of amplifier is the erbium-doped fiber amplifier (*EDFA*) [4–5]. Its operation is based on erbium ion (Er^{3+}) stimulated radiation, which allows signals to be amplified in the wavelength range 1530–1565, where *EDFA* amplifiers are used in *WDM* communication systems due to their high reliability and compatibility with existing infrastructure. However, with increasing demands on *WDM* systems – increasing channel numbers, data transmission speeds, and line lengths – the limitations of traditional *EDFAs* have become apparent. These include limited gain bandwidth, reduced efficiency at high pump powers, and difficulties in providing uniform gain across multiple channels over a wide spectral range. To overcome these problems, co-doped amplifiers based on *SMF* fiber doped with Er^{3+}/Yb^{3+} ions are being actively developed. Such fiber has several significant advantages. Ytterbium (Yb^{3+}) has a broad absorption band in the 900–1060 nm range and efficiently converts pumping energy into erbium ion excitation. This energy transfer scheme significantly increases amplification efficiency, especially at a wavelength of 980 nm. As a result, Er^{3+}/Yb^{3+} doped amplifiers (*EYDFAs*) provide higher output power, lower nonlinear effects, and more stable operation in multi-channel communication systems.

Due to these advantages, broadband *EYDFA* amplifiers are becoming an integral part of modern optical fiber communication systems, including dense wavelength division multiplexing (*DWDM*) and coarse wavelength division multiplexing (*CWDM*) [6]. They enable increased transmission distances without signal regeneration, improved network energy efficiency, and more uniform channel amplification. In addition, advances in active fiber manufacturing technology and optimization of *EYDFA* spectral characteristics are creating the conditions for their integration into new areas of optical networks – high-speed trunk lines, submarine cable systems, data processing centers, and *5G/6G* infrastructure.

Thus, the research and development of Er^{3+}/Yb^{3+} doped optical fiber amplifiers is a pressing scientific and technical task. These devices provide fundamental opportunities for the future development of high-capacity and energy-efficient optical communication systems, which form the basis for next-generation global telecommunications networks [7].

The current applicability of optical signal amplification technology is highly relevant in integrated photonic devices, that employ optical microspheres to generate optical signals via the nonlinear Kerr effect. [8]. The main reason is that the signal is generated using a frequency comb in discrete frequency lines spaced at equal intervals. This structure ensures accurate and stable frequency generation, resulting in a coherent light source with spectrally limited lines. These spectrally limited lines are obtained thanks to the stable generation of the frequency comb and low phase noise, which ensures that the generated signals are monochromatic and have low frequency fluctuations [9]. The role of the Kerr effect in this process is related to the use of a single light source. Thanks to this nonlinear process, it is possible to form several comb lines that are closely spaced at a certain distance from each other and "locked" in phase (no phase shift), thus obtaining narrow spectral lines in the optical frequency comb [10].

The pulse position modulation (*PPM*) technique is used in communication systems to increase energy efficiency and reduce signal attenuation in data transmission [11]. *PPM* information is encoded by the pulse position in the time window, which reduces the impact of noise and nonlinear distortion. *EDFA* amplifiers are used, which amplify the signal without the need for optoelectronic conversion, preserving the pulse phase and amplitude structure. This ensures high receiver sensitivity and increases transmission distance and spectral efficiency, which is particularly important for high-capacity multi-channel *DWDM* systems. The use of *PPM* in optical fiber networks remains a promising area, especially for energy-efficient and highly reliable next-generation optical communication channels [12, 13].

The aim and the Doctoral Thesis

Summarizing the above facts about the development trends of fiber optic transmission systems, the goal of the doctoral thesis was set: To develop and evaluate a double-clad Er^{3+}/Yb^{3+} doped fiber optical amplifier, electrical 50 ps pulse expansion and lens fiber technology for high-speed optical fiber communication systems and integrated photonic devices.

In order to achieve the set aim, the following theses were put forward for the defence of the Doctoral Thesis.

1. Using a 40-channel *DWDM* communication system with the developed Er^{3+}/Yb^{3+} doped fiber optical amplifier model and applying the cladding pumping technique in the fiber, the smallest gain difference ($\Delta G < 9$ dB) can be achieved at a fiber length of 7 m.

2. By using reference pulse position modulation (TR-PPM) signals with an input pulse duration of 50 ps and *TR-PPM* signal demodulation with a developed low-pass filter (*LPF*), it is possible to ensure electrical pulse expansion to at least 700 ps.

3. For integrated photonic devices, using a separated SMF-28 fiber end and a single-mode optical lens, it is possible to achieve the lowest connection point losses at a lens diameter of 129 μm.

The main tasks of the Doctoral Thesis

In order to achieve the set goal of the Doctoral Thesis and prove the proposed theses, it is necessary to perform the following tasks.

1. In a simulation scenario, evaluate the average gain, noise factor, and gain difference between channels in a *WDM* 64-channel communication system with double-clad Er^{3+}/Yb^{3+} alloyed fibers, depending on the *EYDF* wavelength and signal propagation direction.

2. Experimentally and in a simulation environment, evaluate the gain coefficient of double-clad Er^{3+}/Yb^{3+} alloyed fiber at an input power of –20 dBm/per channel in a *WDM* 40-channel communication system, depending on the pumping power and *EYDF* wavelength.

3. Develop a hybrid *RA-FOPA* and single-pump-source *FOPA* amplifier, evaluate its performance in a 16-channel *DWDM* communication system with 10 Gbit/s data transmission per channel, without exceeding the received signal $BER \geq 1\times10^{-9}$ threshold.

4. Using transmitted reference pulse position modulation (*TR-PPM*) signals with a pulse duration of 50 ps and a full width of half maximum (*FWHM*), evaluate pulse broadening with several types of fabricated *LPF*.

5. In integrated photonic devices, evaluate the connection losses for specific lens fibers across the entire 1550 nm wavelength range.

THESIS APPROVAL AND PUBLICATIONS

The results of the Dctoral Thesis are presented in eight scientific articles and conference proceedings included in databases of journals or collections of articles (SCOPUS, WoS, IEEE) The results of the Thesis have been presented at five conferences.

1. Olonkins, S., Supe, A., Bobrovs, V., and **Prigunovs**, D. "Comparison of Single-pump FOPA and Raman Assisted FOPA Performance in a 16 Channel DWDM Transmission System," 2019 Photonics & Electromagnetics Research Symposium – Fall (PIERS – Fall), Xiamen, China, 2019, pp. 723–727, doi: 10.1109/PIERS-Fall48861.2019.9021339.

2. **Prigunovs, D**., Kudojars, R., Morevs, P., Parfjonovs, M., Supe, A., Matsenko, S., Krotov, A., Redka, D., Bobrovs, V., Salgals, T. Design and Evaluation of Rare-Earth-Doped Fiber Amplifier for WDM-PON Transmission Systems. In: 2024 Photonics & Electromagnetics Research Symposium (PIERS 2024), China, Chengdu, 21–25 April 2024. doi:10.1109/PIERS62282.2024.10618170.

3. Spolītis, S., **Prigunovs, D**., Migla, S., Ortiz Blanco, D., Šēlis, O., Šics, P., Ostrovskis, A., Solovjova, T., Semeņako, J., Āboltiņš, A. Demonstration of 512-TR-PPM Fiber Optical Transmission Link. In: 2023 Photonics & Electromagnetics Research Symposium (PIERS 2023), Czech Republic, Prague, 3–6 July 2023, doi:10.1109/PIERS59004.2023.10221307.

4. Sedulis, A., Ostrovskis, A., Zaķis, K., Rubuls, K., Ortiz Blanco, D., **Prigunovs, D**., Alnis, J., Bobrovs, V., Spolītis, S. Fabrication of Lensed Fibers with Arc Fusion Splicer for Telecommunication Applications. In: 2023 Photonics & Electromagnetics Research Symposium (PIERS 2023)*:* Proceedings, Czech Republic, Prague, 3–6 July 2023, doi:10.1109/PIERS59004.2023.10221315.

5. Sedulis, A., Žurikovs, D., Rubuls, K., Murans, I., **Prigunovs, D**., Salgals, T., Ortiz Blanco, D., Parfjonovs, M., Ģēģere, L., Ostrovskis, A., Ozoliņš, O., Bobrovs, V., Spolītis, S. Development and Assessment of a Lensed Fiber for Applications in Integrated Photonics. No: 2024 Photonics & Electromagnetics Research Symposium (PIERS 2024), China, Chengdu, 21–25 April 2024, doi:10.1109/PIERS62282.2024.10618517.

The results of the Doctoral Thesis are presented in three scientific articles and conference proceedings included in databases of journals or collections of articles (indexed in SCOPUS, WoS, IEEE).

1. Supe, A., Olonkins, S., Udaļcovs, A., Gegere, L., Murnieks, R., **Prigunovs, D**., Seņkans, U., Grube, J., Elsts, E., Spolitis, S., Ozoliņs, O., Bobrovs, V. "Cladding-Pumped Erbium/Ytterbium Co-Doped Fiber Amplifier for C-Band Operation in Optical Networks". Applied Sciences, 2021, Vol. 11, No. 4, Article number 1702. ISSN 2076-3417. Available from: doi:10.3390/app11041702.

2. Zakis, K., Olonkins, S., Udalcovs, A., Lukosevics, I., **Prigunovs, D**., Grube, J., Bikse, L., Supe, A., Ozolins, O., Spolitis, S., et al. "Cladding-Pumped Er/Yb-Co-Doped Fiber Amplifier for Multi Channel Operation". Photonics, 2022, 9,457. doi:10.3390/photonics9070457.

3. Solovjova, T., Semenako, J., **Prigunovs**, D., Ortiz, D., Spolitis, S., Aboltins, A. "Picosecond Pulse Expansion Using the Low-Pass Filter in Event Timer-Based PPM Communication System,"2022 Workshop on Microwave Theory and Techniques in Wireless Communications (MTTW), Riga, Latvia, 2022, pp. 29-34, doi: 10.1109/MTTW56973.2022.9942566.

INTRODUCTION

Nowadays, *WDM* communication systems are increasingly being introduced, and several studies are actively being conducted on the development of components for such systems and the improvement of their performance [14–16]. *WDM* communication systems allow for a much more efficient use of optical fiber resources compared to alternative technologies [17].

The data transmission speed in *WDM* communication systems is increased by assigning a separate wavelength to each channel, thus transmitting multiple channel signals simultaneously in a single optical fiber. To increase the number of channels, multiplexing and demultiplexing components are required, whose introduced attenuation significantly reduces the signal power [18–20]. Furthermore, despite the fact that the attenuation of optical fiber in the C-band wavelength range is only 0.2 dB/km, it accumulates as the signal propagates through the optical fiber and significantly limits the transmission distance because the sensitivity of the photodetector at the receiver end is limited. Therefore, it is necessary to compensate for the attenuation of the transmitted signal [21]. The attenuation of the transmitted signal can be compensated for by using signal regenerators or optical amplifiers. A regenerator is a complex device that includes both electronic and optical components. It must detect the transmitted optical signal, convert it into an electrical signal, process it, and regenerate it with the help of an optical transmitter [22, 23]. The use of optical signal regenerators in modern *WDM* communication systems is an economically disadvantageous and complex solution, as it requires the demultiplexing, reception, processing, and regeneration of all transmitted channel signals. The use of single-channel *WDM* regenerators is also not economically efficient, as there is an alternative approach to compensating for optical losses. Optical amplifiers allow simultaneous amplification of multiple transmitted channel signals without demultiplexing and additional operations. Compared to the use of signal regenerators, the use of optical amplifiers is an effective way to compensate for the power loss of transmitted signals, which in the case of *WDM* communication systems allows for a significant reduction in costs as the number of system channels increases. It is also an economically advantageous solution for single-channel *WDM* systems compared to regenerator solutions [24].

Multimode double-clad erbium-doped fiber amplifiers are widely used in *SDM* networks because they have low energy conversion efficiency. To address this issue, the use of ytterbium (Yb^{3+}) and erbium (Er^{3+}) amplifiers with co-propagating is considered an effective approach [25, 26].

However, this changes the gain profile of the Er^{3+} doped fiber amplifier and causes a gain difference between optical wavelengths in the C-band, significantly limiting the effective bandwidth of dense wavelength division multiplexing (*DWDM*) systems.

Erbium (Er^{3+})/ytterbium (Yb^{3+}) amplifiers have complex characteristics, particularly with regard to the gain profile and pumping conversion efficiency. These parameters depend on the alloyed fiber profile, absorption/emission spectra, and input signal power. Based on this information, in order to meet the ever-increasing demand for higher network capacity, conventional *EDFAs* will need to be replaced by alternative amplification solutions.

Fiber optic parametric amplifiers (*FOPAs*) are innovative types of amplifiers that can be considered one of the possible alternatives to traditional *EDFAs*. The characteristics of *FOPA* amplification show why this type of amplifier is likely to be widely used around the world in the near future: available scientific publications indicate that amplifiers of this type can provide amplification of up to 70 dB [27] and an amplification bandwidth of up to 270 nm [28, 29].

In addition to their remarkable *FOPA* amplification properties, they offer a range of additional applications for all-optical signal processing, such as wavelength conversion using the idle spectral components generated by four-wave mixing, dispersion compensation using phase conjugation, optical signal regeneration in the middle of the transmission path, and modulation format conversion [30–33]. The performance of *FOPA* is significantly affected by several factors, such as high amplification sensitivity to phase mismatch of interaction spectral components, stimulated Brillouin scattering (*SBS*), relative intensity noise, four-wave mixing (*FWM*) caused by interchannel overlap with bidirectional pumping in the case of *FOPA*, and stimulated Raman scattering (SRS) [34]. Ignoring the negative impact on SRS, the nonlinearity of this fiber can be used to increase the performance of *FOPA* using a unidirectional pumping light source during amplification for parametric amplifier pumping, which requires additional power to initiate the necessary nonlinearity. The other nonlinearities mentioned above are significant in high-speed data transmission systems, but *FWM* is highly dependent on the distance between channels. Reducing this effect increases *FWM*. Unlike other nonlinearities, *FWM* could cause power loss and degrade the performance of *DWDM* systems [35].

Optical signal amplification technologies are highly relevant for integrated photonic devices that employ optical microspheres to generate optical signals via the nonlinear Kerr effect. [8]. The main reason is that the signal is generated using a frequency comb in discrete frequency lines spaced at equal intervals.

This structure ensures accurate and stable frequency generation, resulting in a coherent light source with spectrally limited lines. These spectrally limited lines are obtained thanks to the stable generation of the frequency comb and low phase noise, which ensures that the generated signals are monochromatic and have low frequency fluctuations [9]. The role of the Kerr effect in this process is related to the use of a single light source. Thanks to this nonlinear process, it is possible to create several comb lines that are closely spaced at a certain distance from each other and “locked” in phase (no phase shift), thus obtaining narrow spectral lines in the optical frequency comb [10].

Pulse position modulation (*PPM*) is used in optical fiber transmission systems, including *DWDM* communication systems, to increase energy efficiency and reduce signal attenuation in data transmission [11]. *PPM* information is encoded by the pulse position in the time window, which reduces the effects of noise and nonlinear distortion. *EDFA* amplifiers are used, which amplify the signal without the need for optoelectronic conversion, preserving the pulse phase and amplitude structure. This ensures high receiver sensitivity and increases transmission distance and spectral efficiency, which is particularly important for high-capacity multi-channel DWDM systems. The use of *PPM* in optical fiber networks remains a promising area, especially for energy-efficient and highly reliable next-generation optical communication channels [12, 13].

1. DOUBLE-CLAD WITH DIFFERENT RARE EARTHS Er^{3+}/Yb^{3+} AND CLADDING-PUMPED FIBER AMPLIFIER EVALUATION IN DWDM COMMUNICATION SYSTEM

Space division multiplexing (SDM) attracts the attention of optical amplifiers pumped with a cladding due to their low pumping power conversion efficiency. To solve this problem, an effective approach is considered to be an erbium (Er^{3+}) and ytterbium (Yb^{3+}) ion-doped optical amplifier with a direct pumping direction. However, they change the gain profile of the Er^{3+} doped fiber amplifier and cause a gain difference in the C-band, significantly limiting the effective bandwidth of dense wavelength division multiplexing (*DWDM*) systems. This chapter is devoted to a detailed study of Er^{3+}/Yb^{3+} cladding-pumped fiber amplifiers (*EYDFAs*) using numerical simulations to determine the most suitable *EYDFA* configuration that provides the desired performance for *WDM* communication system applications.

Double-clad *EYDFA* fibers were used in the simulation model, and the simulation results were compared with experimental results. The following amplifier characteristics were studied for different fiber lengths, channel numbers, and input signal power levels: gain coefficient, gain uniformity, and noise factor.

Cladding-pumped erbium (Er^{3+})/ytterbium (Yb^{3+}) rare ion-doped fiber amplifiers are more effective at high output powers, but this amplification technique also has potential in telecommunications applications. Amplifiers of this type have complex characteristics; in particular, the amplification profile and pumping conversion efficiency must be taken into consideration. These parameters depend on the doped fiber profile, absorption/emission spectra, and input signal power. In this context, a prototype of an Er^{3+}/Yb^{3+} ion-doped fiber amplifier (*EYDFA*) with cladding pumping was developed and investigated. The aim of this model was to optimize the *EYDFA* configuration (doped fiber length, pumping power, input signal power) suitable for signal amplification in a multi-channel optical fiber transmission system with dense wavelength division in the C-band (1530–1565 nm). This approach involves experimentally determining the parameters of Er^{3+}/Yb^{3+} doped fiber using a simulation configuration to determine the initial *EYDFA* configuration before performing experimental measurements.

The experimental *EYDFA* prototype was tested under various scenarios using a 48-channel dense wavelength division multiplexing (*DWDM*, 100 GHz) system to evaluate the

absolute gain and gain stability. The results obtained allow assessment of the suitability of the cladding pump amplifier for broadband signal amplification.

1.1. Description of the simulation model of an optical amplifier with double-clad $Er3^{+}/Yb3^{+}$ doped fibers

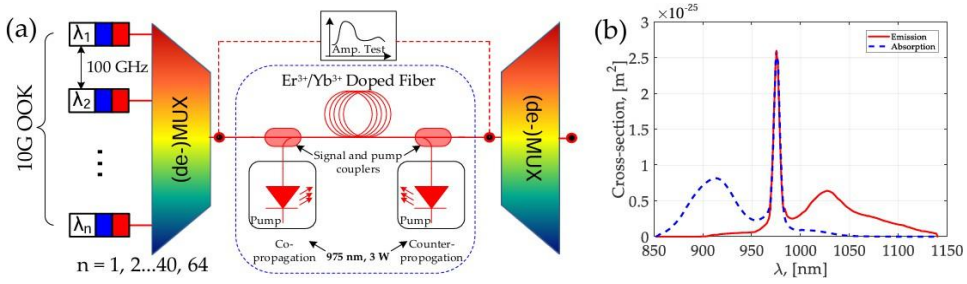

Fig. 1.1. (a) – Simplified simulation model of cladding pumped *EYDFA*; (b) – Er^{3+}/Yb^{3+} absorption and emission cross sections measured for $Er(^{3+})/Yb(^{3+})$ doped fiber using a spectrum measurement method and entered into the simulation model.

The simulation model was implemented using VPIphotonics Design Suite [VPIphotonics], while the absorption and emission cross-sections of Er^{3+}/Yb^{3+} phosphosilicate glass fibers with double cladding were experimentally measured at the ŠOPS laboratory and entered as input data for the simulation configuration (see Fig. 1.1 (b)). Thus, the configuration consists of three parts:

i) *n* 10 Gb/s OOK WDM transmitters;

ii) A realistic model of the *EYDFA*, consisting of the *EYDFA* itself, an optical pumping light source (central wavelength λp = 975 nm at 25 °C and output power 3–5 W), a high-power optical combiner/splitter and amplifier test block to evaluate its characteristics (e.g., gain spectrum and noise figure (NF));

iii)WDM (de-)multiplexers and receivers for signal quality evaluation.

The main component of this optical direct connection (*OB2B*) setup is the optical fiber model. For this experiment, a double-clad Er^{3+}/Yb^{3+} fiber with a direct pumping direction from VPIphotonics Design Suite simulation software was used. According to its description, this model is based on two-way signal propagation equations and multi-level ion population velocity equations. This model was adapted to *EYDF*, where measured cross-sections were used, as well as refined emission and absorption spectra and overlap coefficients to refine the coupling and propagation of the *WDM* signal (~ 1550 nm) and pump signal (~ 975 nm) (which depends on the fiber profile and dimensions). The simulation model was studied using bidirectional signal pumping, considering several aspects such as $Er3^{+}/Yb3^{+}$ ion energy

transfer, transverse relaxation effects, excited state absorption, Rayleigh scattering, and Kerr nonlinearity. The values of the setup parameters are shown in Table 1.

Table 1

Amplifier setting parameters

System parameters	
Bitrate and modulation	10 Gbps *NRZ-OOK*
Number of channels (*n*)	1–64
The carrier frequency of the first/last channel	191.60 THz
Channel spacing	100 GHz
Single channel power	-25 dBm/channel to -10 dBm/channel
EYDFA pump parameters	
Pump wavelength	975 nm at 25 °C temperature
Pump power	3 W, operational range 0.3–5 W
Pumping direction	Co-/counter propagation
Doped fiber parameters	
Length	1–10 m
$Er(3^+)$ concentration	1×10^{25} m^{-3}
$Yb(3^+)$ concentration	2×10^{26} m^{-3}
$Er3^+/Yb3^+$ cross-relaxation coefficient	1×10^{-22} m^3/s
Core area/inner cladding area ($A_{core}/A_{inner\ cladding}$)	0.0058
Inner cladding area/outer cladding area ($A_{inner\ clading}/A_{outer\ cladding}$)	0.9203

The simulation model included parameters that define both the *WDM* system and the *EYDFA* under test. In this case, a 10 Gb/s *NRZ-OOK* signal was used, with center frequencies located in the C-band (1530–1565 nm), using a 100 GHz grid with a total number of channels up to $n = 64$; channels 41–64 are outside the C-band (fc > 195.6 THz). Amplifiers of this type are used to obtain the dependence of the amplifier gain and noise figure characteristics on wavelength, especially for high (> 10 dBm/per channel) and low (< 25 dBm/per channel) input signal power.

The category "*EYDFA* pumping parameters" provides more detailed information on the optical pumping light source and its direction in relation to signal propagation. Finally, the category "Alloyed fiber parameters" includes the measured, calculated, and given

characteristics of *EYDF*, which were used to create a model of *EYDFA* in fiber optics transmission system (*FOTS*) laboratory.

1.2. Evaluation of a double-clad Er^{3+}/Yb^{3+} doped fiber simulation model in a 64-channel DWDM communication system

In this section, *EYDFA* configuration parameters such as the length of the Er^{3+}/Yb^{3+} doped fiber, its absorption and emission cross sections, and the direction of the pumping signal were evaluated, as well as the influence of wavelength-dependent properties, gain flatness, noise figure, and maximum output power. Before evaluating the power reduction caused by the *EYDFA*, its performance was characterized at several wavelengths by varying the number of *DWDM* channels and their power levels. The purpose of this simulation study was to find the most suitable amplifier configuration that causes the least distortion while providing the smoothest possible gain spectrum. This analysis used an optical pump light source operating at λp = 975 nm and 3 W output power.

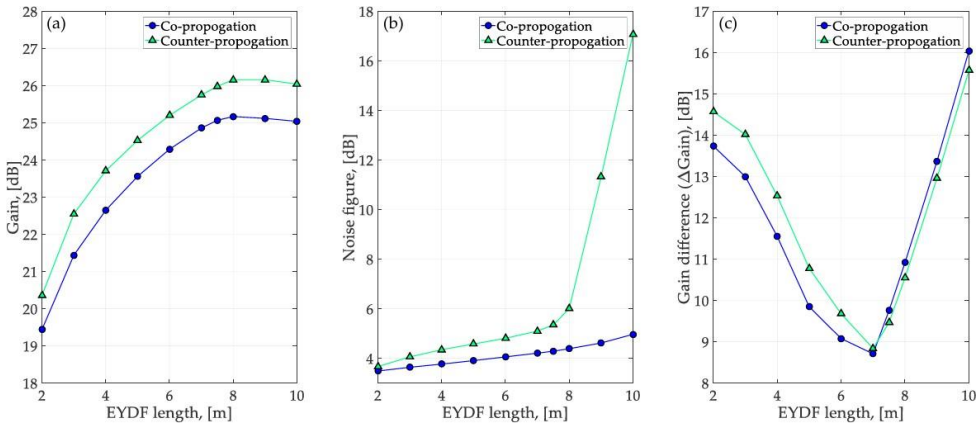

Fig. 1.2. (a) Average gain, (b) average noise figure, and (c) maximum gain difference between channels as a function of *EYDF* length in a system with 40 *WDM* channels, input signal power –20 dBm per channel with 3 W 975 nm direct (blue) and reverse (green) pumping sources.

These configuration values were selected based on the specifications of the *FOTS* laboratory high-power light source, and the direction of the pumping signal propagation was considered – forward and backward pumping. To choose the *EYDF* length and the direction of the pumping signal, curves obtained from a 40-channel *WDM* system were used, showing the

change in the amplifier gain coefficient, noise coefficient, and maximum output power dependence on the *EYDF* length (see Fig. 1.2).

The results obtained show that the maximum amplification was achieved at an *EYDF* length of 8 m, regardless of the direction of the pumping signal (see Fig. 1.2 (a)). A longer *EYDF* does not provide greater amplification, which can be explained by the depletion of the pumping radiation. Further increasing the length of the cladding fiber not only fails to produce additional amplification but also causes the amplified signal power to decrease due to the attenuation of the *EYDF* itself. The amplifier becomes noisier, especially in a configuration where the signal is pumped in the opposite direction to the pumping direction (see Fig. 1.2 (b)). In this case, the noise factor is no greater than 4.5 dB (direct pumping) and 6 dB (reverse pumping). Figure 1.2 (c) shows the maximum gain difference observed between channels 1 and 40 (Ch1–Ch40) in a 40-channel *DWDM* system with an optical input power of –20 dBm/channel. Gain uniformity is an important feature in systems with multiple alloy fiber lengths. If all *DWDM* channels were not amplified equally, the power difference would increase with each range, limiting the maximum transmission distance. The smallest gain difference ($\Delta G < 9$ dB) is obtained for a 7 m long EYDF for both 975 nm pumping signals in direct and reverse pumping. It is significantly larger for shorter and longer *EYDF* segments, indicating that in this particular combination of pumping power (3 W) and *EYDF* length (7 m), an adequate level of ion population inversion was achieved, and therefore these parameters remain unchanged.

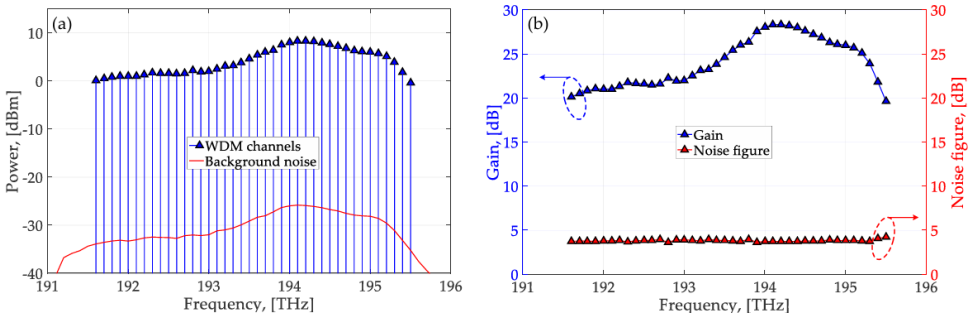

Fig. 1.3. (a) – Optical spectrum obtained at the *EYDFA* output with a 7-meter-long alloy fiber; and (b) – average gain and noise figure in a system with 40 WDM channels, input signal power
–20 dBm per channel and with 3 W 975 nm direct (blue) and counter-directional (green) pumping sources.

Finally, it was decided to use a pumping signal with a reverse pumping direction, so a lower noise coefficient was chosen rather than higher amplification. Figure 1.3 (a) shows the output power spectrum, while Fig. 1.3 (b) shows the individual gain and noise factor of each

EYDFA-amplified *DWDM* channel. Due to the amplifier gain and noise figure depending on the wavelength, the output spectrum is not flat. The amplifier output power levels vary from 0.1 dBm to 8.3 dBm per channel (dBm/per channel, see Fig. 1.3 (a)), resulting in a gain difference of 19.7–28.3 dB and a noise figure of 3.7–4.2 dB, see Fig. 1.3 (b). The input optical power (pIN) for all 40 *WDM* channels examined was set at –20 dBm/per channel.

Next, the characteristics of *EYDFA* (gain, maximum gain difference, and noise coefficient) were studied under various operating conditions by changing the number of *DWDM* channels and their optical power levels.

During the analysis of the results, *DWDM* configurations with 1, 2, 4, 8, 16, 32, 40, and 64 channels were examined, where the input power levels were set from –25 to –10 dBm/per channel, see Fig. 1.4.

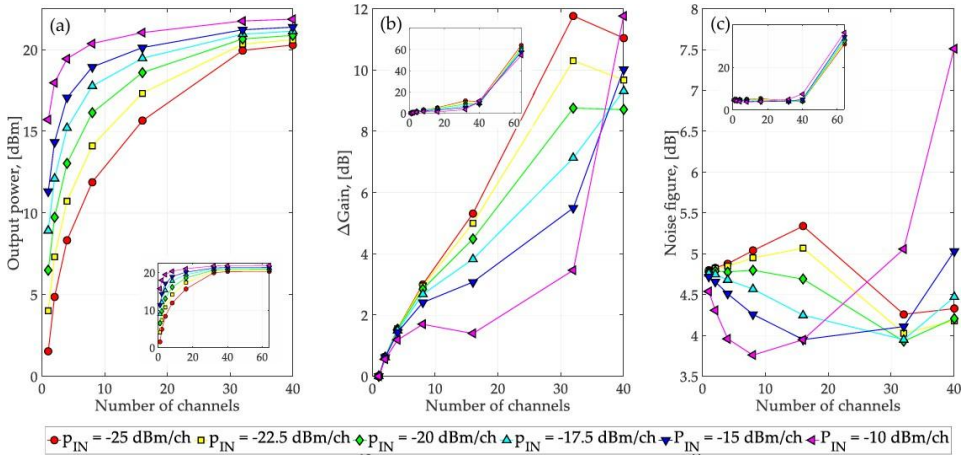

Fig. 1.4. (a) – Output power, (b) – maximum gain margin, and (c) – maximum noise figures versus number of *WDM* channels and their input power for an *EYDFA* configuration with a 7-meter-long *EYDF* and P_{pump} = 3 W at λ_{pump} = 975 nm for forward pumping.

The output power curves show that the greater the number of *DWDM* channels, the smaller the output power difference. The amplifier becomes saturated and ultimately cannot amplify more than 40 *DWDM* channels, even if its power is only 25 dBm/channel.

When analyzing the output power curve at pIN = 25 dBm/channel, it was noticed that the output power level increases by 3.5 dB when the number of *DWDM* channels is increased from two to four. However, the corresponding figure is 4.3 dB when the number of *DWDM* channels is increased from 16 to 32 channels. This behavior indicates that low-power optical signals (i.e., with low input power and/or a small number of channels) are unable to fully utilize the population inversion that occurs in the gain medium. Consequently, the unused portion of population inversion ultimately results in excessive amplified spontaneous emission (*ASE*) noise, which causes poor noise figure (see Fig. 1.4 (c)). In contrast, high input power consumes the gained population inversion, so that the gained amplification decreases and the output power reaches its limit. The output power increases by 0.3 dB when eight additional channels are added to a 32-channel *DWDM* system (pIN = 25 dBm/per channel), and remains similar even when the number of channels is increased to 64. Higher pump signal power does not necessarily mean higher gain or higher output power. Even when using a 4 W pump signal, in a 40-channel configuration with pIN = 20 dBm/channel, the output power increases by no more than 0.2–0.3 dB. Consequently, the maximum output power of the proposed *EYDFA* is limited to approximately +22 dBm. The maximum gain difference curves (see Fig. 1.4 (b)) show the following trend: the higher the input power, the lower the gain difference in a DWDM system with 4–32 channels. The main reason is that in order to achieve a similar gain level for signals with higher input power, a larger portion of the population inversion is consumed. At a given population inversion level, optical signals with higher power are less amplified and the gain difference between channels becomes smaller. However, for 40 *DWDM* channels, the opposite situation occurs, where the gain difference becomes larger when the input signal power is higher (for example, comparing the –25 dB/per channel and –10 dBm/per channel curves). This behavior occurs because higher power signals more effectively deplete the ion population inversion. Increasing the number of *DWDM* channels to 40 at 25 dBm input signal changes the average population inversion level across the *EYDF* to a value that provides more uniform gain across the transmission system frequency band. More uniform amplification (gain) of all 40 *DWDM* channels was observed at pIN = 25 dBm/channel, while at 10 dBm/channel the population inversion decays much faster before similar uniformity is achieved. A similar trend can be observed for the *EYDFA* noise factor (see Fig. 1.4 (c)). For channels with pIN – 20 dBm/per channel, the noise factor first decreases with each additional *DWDM* channel until the number of channels (and their total power level) reaches a certain optimal point, beyond which the noise factor begins to increase. With fewer power channels, the noise factor first

increases by 0.5–1 dB and then begins to decrease, reaching 4–4.5 dB for 32–40 *DWDM* channels.

1.3. Simulation and experimental evaluation of a double-clad Er^{3+}/Yb^{3+} doped fiber amplifier model in a 48-channel DWDM communication system

This section describes the simulation model used to evaluate the expected key performance indicators at different fiber lengths. The experimental model of the amplifier under test is also described here, and the simulation and experimental results are compared. The simulation scheme was created using VPIphotonics Design Suite [36], which is shown in Fig. 1.5. The input signal consists of 48 channels with a 100 GHz channel spacing and 37.5 GHz bandwidth corresponding to the settings of the possible *WSS*. This optical carrier signal containing 48 channels emulates optical carriers (modulated signal data channels in a *WDM* solution) (see Fig. 1.5).

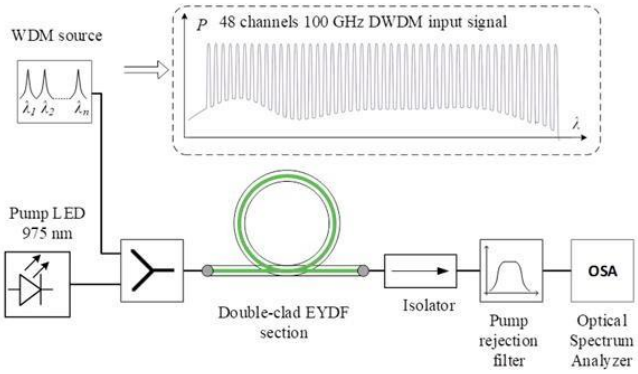

Fig. 1.5. Simulation of *EYDFA WDM* 48-channel model, with cladding pumping technique.

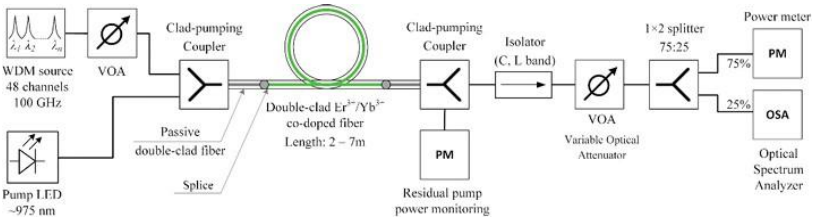

Fig. 1.6. Experimental cladding-pumped *EYDFA WDM* 48-channel model.

The purpose of the simulation model is to determine the amplification characteristics and provide the base values for the *EYDF* length and pumping parameters for the experimental configuration. The simulation model [37] was further improved using the laboratory prototype

shown in Fig. 1.6. where the amplification of a 3 m long fiber was measured. Accordingly, a fictitious (data-unmodulated wavelength) *WDM* signal was obtained, consisting of 48 channels with a bandwidth of 37.5 GHz and spaced 100 GHz apart, as shown in the inset of Fig. 1.5. A high-power multimode diode stabilized at 30 °C with a bandwidth of 6 nm using a thermoelectric cooler (see Fig. 1.6. was used as the pump light source. This pumping source has a minimum output power threshold of 0.6 W, and active temperature control is important for the diode, as higher temperatures reduce the output power and shift the spectrum to longer wavelengths. The minimum output power threshold for this pumping source is 0.6 W. Active temperature control is important for this diode, as higher temperatures reduce the output power and shift the spectrum to longer wavelengths. It has been found that maintaining a lower diode temperature results in higher *EYDFA* gain. The revised model was then used to evaluate the optimal EYDF length and pumping power for broadband signal amplification, which was used to analyze the results obtained. The main parameters of the *EYDF* used in the simulations are summarized in Table 2.

Table 2

Amplifier setting parameters

System parameters	
Number of channels	48
Channels carrier frequency range	191.35–196.05 THz
Channel spacing	100 GHz
Single-channel power (simulation)	−20 dBm
Single-channel power (experimental)	−25 to −10 dBm
EYDFA pump parameters	
Pump wavelength	973–977 nm at 30 °C
Pump power	0.6–2.5 W
Pump direction	Co-propagating
Doped fiber parameters	
Length	2–7 m
Er^{3+} concentration	$1 \times 10^{-25} m^{-3}/s$
Yb^{3+} concentration	$1 \times 10^{-26} m^{-3}/s$
Er^{3+}/Yb^{3+} cross-relaxation coefficient	$1 \times 10^{-22} m^{-3}/s$
Overlap factor (at 1530 nm)	0.0027
Overlap factor (at 980 nm)	0.9203

It was found that maintaining a lower diode temperature results in greater *EYDFA* amplification than closer to the maximum wavelength of *EYDF* absorption (976 nm). The spectrum of the pumping light source – the diode – was centered at a wavelength around 975 nm, which is ~ 1 nm below the maximum absorption wavelength of *EYDF*. Flat pumping fiber connectors were attached to both ends of the *EYDF*. This was used to separate the pump light from the amplified signal. The optical power at the *EYDF* output was controlled for both pumping and the *DWDM* signal. Finally, the output signal spectrum was analyzed to obtain the gain for each channel. No such significant increase is observed in other wavelength regions of the amplification spectrum, i.e., the amplification profile is uneven.

At a pumping power of 2 W, the *EYDF* length was increased from 3 m to 5 m, an additional 5 dB was obtained in the wavelength range from 1555 nm to 1565 nm, and by increasing the *EYDF* length to 7 m, an additional 2.8 dB was obtained. Figure 1.13 shows that increasing the *EYDF* length increases the output gain in the 1535–1545 nm range, but the gain maximum shifts to longer wavelengths.

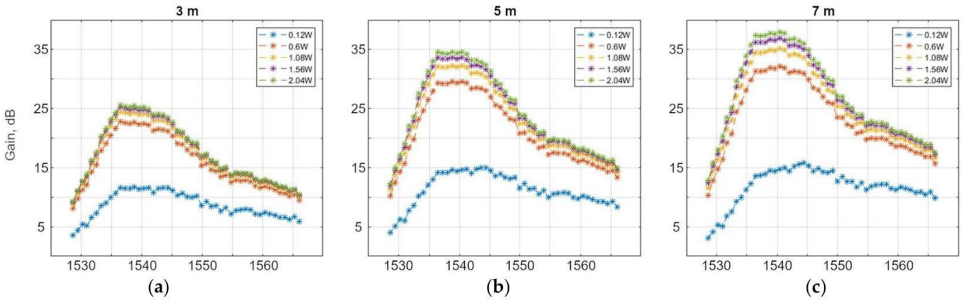

Fig. 1.7. Simulation results with EYDFA gain of –20 dBm/per channel for a 48-channel signal depending on the pumping power (0.12–2 W) at three *EYDF* lengths: (a) 3 m, (b) 5 m, and (c) 7 m.

Figure 1.7 shows that increasing the length of the *EYDF* increases the output gain in the 1535–1545 nm range, but the maximum gain shifts to longer wavelengths. The corresponding gain values are summarized in Table 3. The simulation results show that in the case of a 3 m long *EYDF*, the amplifier produces almost identical gain spectra at 1 W and 2 W pumping power. The corresponding gain values are summarized in Table 3. This means that for relatively short *EYDF* sections, 1 W pumping power is sufficient to ensure inversion of the excited Er^{3+} population and maintain signal amplification. Therefore, pumping powers above 1 W can be considered excessive for such short-doped fiber lengths.

Table 3

Simulation of *EYDFA* Amplification Development

EYDF length, m	3	5	7
Maximum gain, dB	25.6	34.6	38
Maximum peak wavelength, nm	1536.4	1538.8	1540.4
Δ Gain, dB	-	9.1	3.4

In the case of a 3 m long *EYDF*, increasing the pumping power from 1 W to 2 W results in only 0.8 dB of additional gain. However, longer *EYDF* fiber sections provide greater gain increase (2.3 dB and 2.8 dB for 5 m and 7 m long *EYDF*, respectively).

These results, obtained through simulation, are used as a reference point for selecting the *EYDF* length and pumping power for the simulation configuration. The first test in the FOTS laboratory was performed using a 7 m *EYDFA* fiber length pumped with 3 W of pumping power. The simulation results obtained show a narrower and flatter *EYDFA* gain profile compared to the simulation results; it is shifted to longer wavelengths and has a sharp drop below 1544 nm. Thus, the 7 m *EYDF* fiber is too long for the selected application. Therefore, the measurements are repeated using shorter *EYDF* ranges (5 m, 3 m, and 2 m) to determine a more suitable length for the experimental configuration. A comparison of the experimental and simulation results is shown in Fig. 1.8.

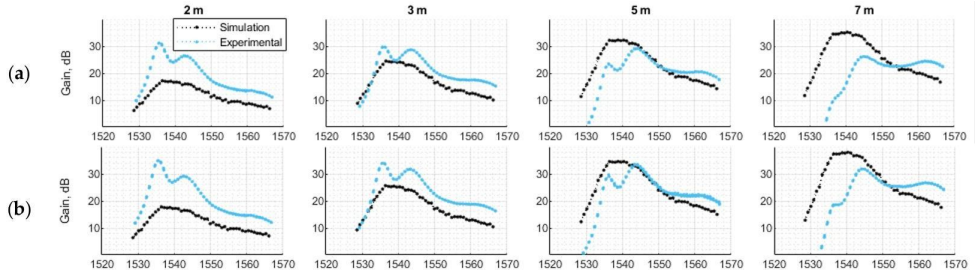

Fig. 1.8. Experimental *EYDFA* gain measurements compared with simulation results at –20 dBm/per channel signal and pump power (a) 1 W and (b) 2 W.

The closest variable is a 3 m long *EYDF* in the 1545–1560 nm wavelength range. Experimental data for longer (5 m and 7 m) *EYDF* sections show signal absorption in the 1530–1540 nm spectral range, which coincides with the $Er3^{+}$ absorption maximum (see Fig. 1.8). This causes additional signal amplification around the wavelength of 1560 nm. This causes additional signal amplification around the wavelength of 1560 nm. Signal reabsorption was not taken into account in the simulation model. The discrepancy between the simulation and experimental data (especially for 2 m) could be related to the specific shape of the *EYDF* inner cladding (and its pumping focusing properties), which is represented in a simplified form as an overlap coefficient in the simulation model. The simulation data cannot be used to accurately describe the amplification shape. These data are useful for determining the initial values of the laboratory equipment. The gain of each channel in the *EYDFA* configuration is analyzed using a 48-channel fictitious *WDM* signal constructed using a broadband *ASE* noise source and *WSS*. After filtering, the signal power level is adjusted with a variable optical attenuator. It should be noted that the number of *DWDM* channels/wavelengths is limited by the *WSS* operating band. The spectra of the cladding-pumped *EYDFA* gain were recorded for configurations with *EYDF* wavelengths of 2 m, 3 m, 5 m, and 7 m, while the signal input power remained unchanged: –25 dBm, –20 dBm, and –10 dBm per channel (see Fig. 1.9).

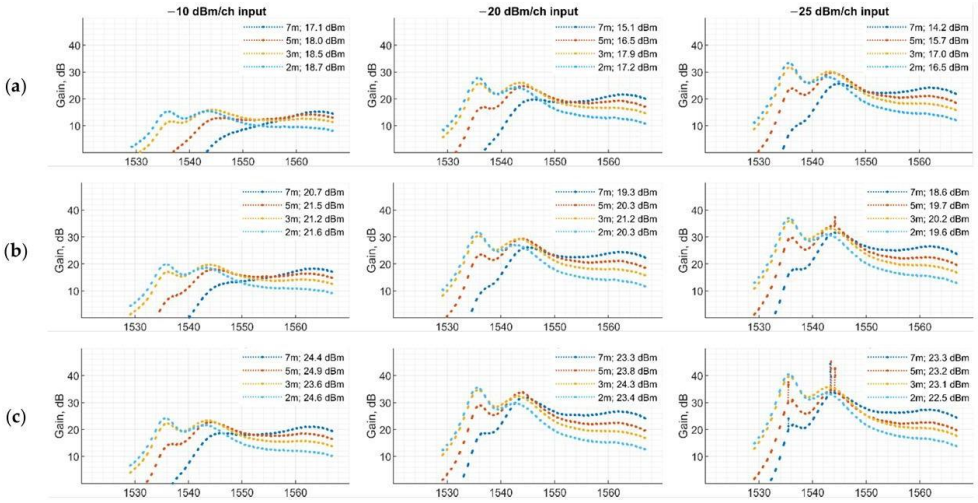

Fig. 1.9. Experimentally measured *EYDFA* gain at three different input signal powers depending on *EYDF* length and pumping power: (a) 0.6 W, (b) 1 W, (c) 2 W. The curve in each graph indicates the fiber length and total output power.

The obtained gain spectra show that with a signal input power of –25 dBm per channel, an undesirable laser radiation maximum was observed at a pumping power above 1 W. At the highest signal input power level (–10 dBm per channel), the usable bandwidth of the amplifier shifts to longer wavelengths as the *EYDF* length increases. At the lowest signal input power level (–25 dBm per channel), increasing the *EYDF* length from 2 m to 5 m, the power levels of the 1544 nm wavelength channels remain almost unchanged (less than 1 dB difference), while the longest wavelengths show significantly higher amplification.

When the *EYDF* length was increased from 5 m to 7 m, channels with wavelengths above 1544 nm were amplified even more. However, for channels with wavelengths around 1536 nm, the gain decreases by 10 dB, and a sharp drop is observed below 1536 nm. This amplification can be explained by $Er3^{+}$ population inversion.

The glow of the pump light comes from the upward luminescence of $Er3^{+}$, which indicates high population inversion. This effect decreases when the input signal is combined with the *EYDFA* amplification signal, as part of the excited Er3+ returns to its ground state, amplifying the C-band signal.

More specifically, the $Er3^{+}$ population inversion [38] required for amplification at these wavelengths is not maintained over the long *EYDF* range, resulting in uneven amplification spectra. In addition, it was observed that the first meter of the *EYDF* glows green when the pumping source is active (see Fig. 1.10).

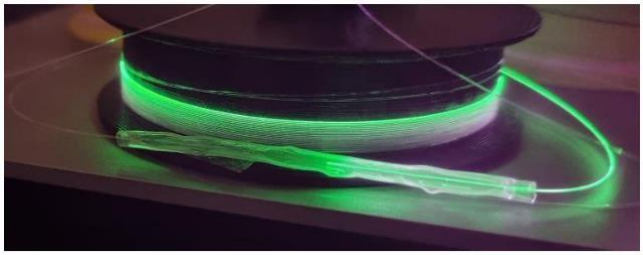

Fig. 1.10. *EYDF* green luminescence with the pumping light source switched on. A purple tint is visible because pumping light leaks from the fiber and is captured by the camera. To avoid the possible effects of thermal expansion, the steel rod has been removed from the protection sleeve of the fusion splice.

2. PERFORMANCE EVALUATION OF OPTICAL FIBER PARAMETRIC AMPLIFIER (FOPA) AND RAMAN-ASSISTED FOPA AMPLIFIER

This chapter compares the performance of the Raman-assisted *FOPA* (*RA-FOPA*) solution with that of a standard single-pump light source *FOPA*, which provides approximately the same amplification level in a 16-channel dense wavelength division multiplexing (*DWDM*) transmission system (see Fig. 2.1). During the research, the main focus was on the total power required by the *FOPA* amplifier to provide a certain level of amplification for the amplified signal quality.

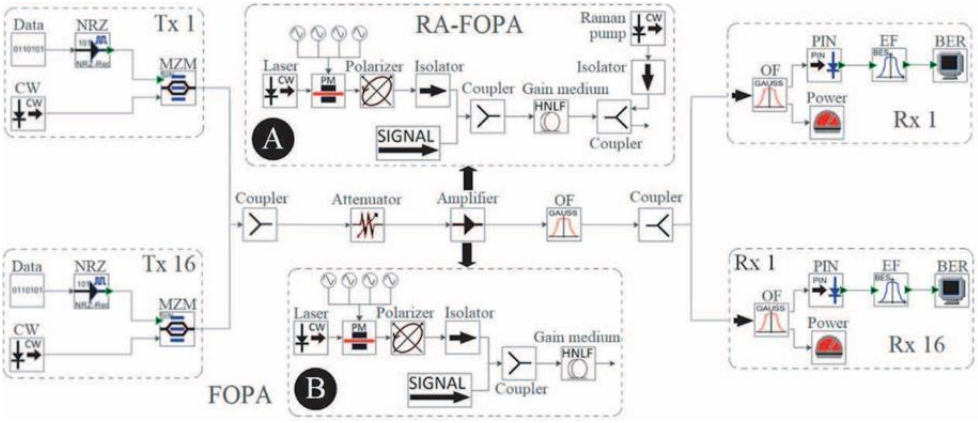

Fig. 2.1. Simulation model of 16 channel 10 Gbps *WDM* transmission system with *NRZ-OOK* modulation format and (a) a *RA-FOPA* preamplifier or (b) a single-pump *FOPA* preamplifier.

2.1. Description of the FOPA simulation model assisted by FOPA and RAMAN in a 16-channel DWDM transmission system

RA-FOPA and single-pump *FOPA* solutions were used as preamplifiers and were placed directly at the attenuator output. After the signal passed through the preamplifier, the amplified signal was sent through a 3 dB bandpass optical filter (*OF*) with a bandwidth of 15 nm and, using an optical splitter with 13.5 dB insertion loss, the transmitted optical signal was split into 16 PIN photodiode-based receivers with a sensitivity of 23.9 dBm at a 10^{-12} bit error rate (*BER*) threshold. At the input of each receiver, the signal passes through a different passband optical filter with a 3 dB bandwidth of 0.11 nm to filter out radiation belonging to adjacent channels. Double filtering is necessary because each filter has a dispersion coefficient of 20 dB, so using a single filter is insufficient to eliminate the effect of residual pump radiation on the quality of the received signal.

In the *RA-FOPA* solution (shown in Fig. 2.1 (a)), 500 mW of 192.92 THz pump output

radiation was sent through a phase modulator used to reduce stimulated Brillouin scattering (*SBS*), an optical polarizer to ensure that the polarization state of the pump matches that of the signal, an optical isolator, and then combined with the signal to be amplified.

The combined signal with a direct pumping direction was then propagated through a 1 km long HNLF with a zero-dispersion wavelength of 1553 nm and a nonlinear coefficient of 15.0 W^{-1} km^{-1}, which is used as an amplification medium and in which the signal amplification took place.

A *Raman* optical amplifier with a pumping power of 500 mW was connected to the other end of the *HNLF*, where the optical signal was transmitted in the opposite direction to the pumping direction relative to the parametric (*RA-FOPA*) pumping signal. This direction of propagation of the Raman pump signal in the *HNLF* was chosen to avoid four-wave mixing (*FWM*) between the Raman and parametric amplifier pumping. The structure of a single-pump *FOPA* solution is similar, but, in this case, there is no Raman pumping, and amplification is provided only by parametric pumping, the power and frequency selection of which is described in the next section.

2.2. Evaluation of the amplification gain spectrum of RA-FOPA and parametric amplified FOPA with a single pumping source

In this section, a simulation model with Raman-assisted *FOPA* and a single pumping laser source *FOPA* solution was investigated, and the results that could provide approximately the same amplification level were analyzed and the two amplification solutions were compared in terms of amplified signal quality. The gain for the 16 channels created by *RA-FOPA* with the configuration described above averages 31.6 dB (from 31.4 dB in channel 1 to 31.8 dB in channel 9). Next, a pumping *FOPA* configuration was obtained that provided approximately the same gain level. The main goal of the experiment was to find a single *FOPA* pumping configuration that would provide amplification in each of the 16 amplified channels and where the channel amplification would not be less than the amplification of the same channel produced by *RA-FOPA*, using the lowest possible pumping power.

The results obtained showed that the lowest pumping power that met the above condition was 755 mW at a pumping center frequency of 192.91 THz. This amplifier configuration provided signal amplification from 31.5 dB (channel 16) to 32 dB (channel 7). The amplification spectrum produced by *RA-FOPA* and single *FOPA* pumping with the parameter configurations described above is shown in Fig. 2.2.

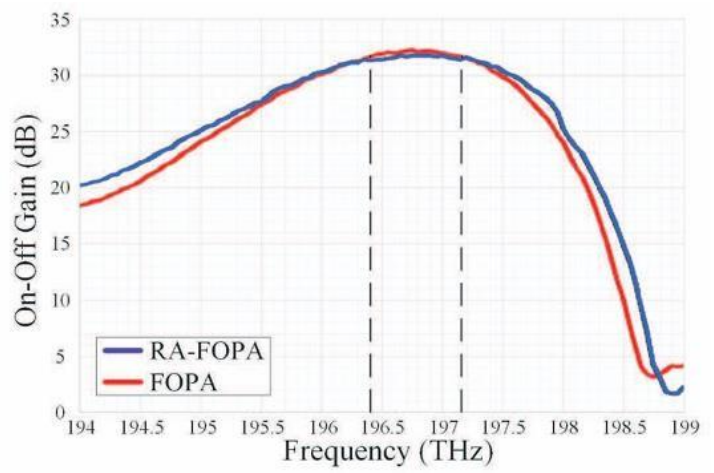

Fig. 2.2. On-off amplification spectrum generated by a single pumping source *FOPA* (red line) and amplification spectrum generated by *RA-FOPA* (blue line).

The gain for the 16 channels created by *RA-FOPA* with the configuration described above averages 31.6 dB (from 31.4 dB in channel 1 to 31.8 dB in channel 9). Next, a pumping *FOPA* configuration was obtained that provided approximately the same gain level.

The main goal of the experiment was to find a single *FOPA* pumping configuration that would provide amplification in each of the 16 amplified channels and where the channel amplification would not be less than the amplification of the same channel produced by *RA-FOPA*, using the lowest possible pumping power. The results obtained showed that the lowest pumping power that met the above condition was 755 mW at a pumping center frequency of 192.91 THz. This amplifier configuration provided signal amplification from 31.5 dB (channel 16) to 32 dB (channel 7). The amplification spectrum produced by *RA-FOPA* and single *FOPA* pumping with the parameter configurations described above is shown in Fig. 2.2.

Comparing the configurations of both amplifier models, it can be seen that the single-pump FOPA solution has a significantly higher amplification efficiency, making it the most suitable in terms of energy consumption to provide approximately the same level of amplification. It requires 245 mW less pumping power than the *RA-FOPA* solution. However, as the results presented later in this chapter will show, *RA-FOPA* has several advantages over standard single-pump *FOPA*.

The results obtained in Fig. 2.2 clearly show the advantage of the *RA-FOPA* solution, as the –3 dB bandwidth of the *RA-FOPA* amplification spectrum is approximately 0.1 THz wider than that of the single-pump *FOPA* amplification spectrum.

2.3. Optical signal-to-noise ratio (OSNR) evaluation in RA-FOPA and single-pump parametric FOPA amplifiers in a 16-channel DWDM system

To evaluate the amount of noise generated by the performance of both amplifiers, the optical signal-to-noise ratio (*OSNR*) at the receiver input was obtained and compared for each of the 16 channels.

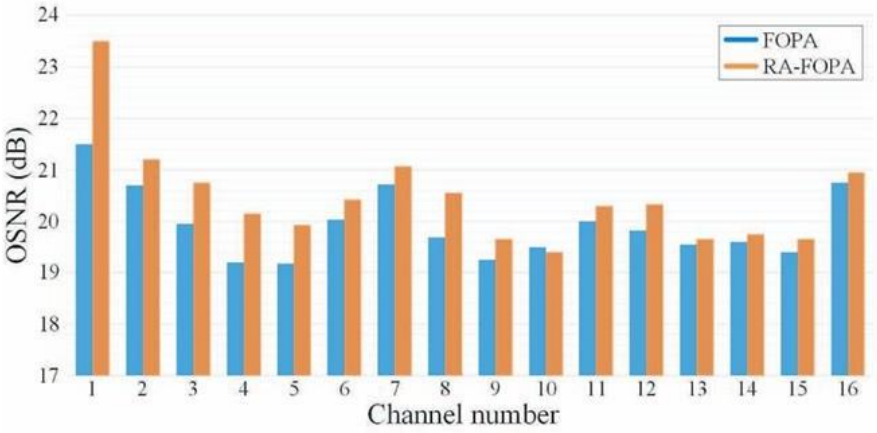

Fig. 2.3. *OSNR* values of the signal received in each channel, obtained in a system with a single pumping FOPA (blue) and in a system with an *RA-FOPA* solution (orange).

The results obtained in Fig. 2.3 clearly show that the *OSNR* values observed in the *RA-FOPA* system are higher in all channels except for channel 10, where the *OSNR* in the standard FOPA system with a single pump source was 0.1 dB higher than in the *RA-FOPA* system (19.4 dB and 19.5 dB, respectively). The largest *OSNR* difference between the two systems was observed in channel 1, where the difference reached 2 dB, but on average, the *OSNR* in the *RA-FOPA* system was 0.8 dB higher than in the system with a single-pumping *FOPA*.

2.4. Bit error rate evaluation of RA-FOPA and single-pumping source parametric FOPA amplifier 16-channel DWDM system

To evaluate the quality of the amplified signal, the *BER* value was obtained depending on the detected signal power in the channel with the highest *BER* (channel 9) in both the *RA-FOPA* system and the single-pump *FOPA* system. It is important to note that the BER values

were not obtained during the experiments but were calculated based on the *OSNR* values. The obtained *BER* dependencies are shown in Fig. 2.4.

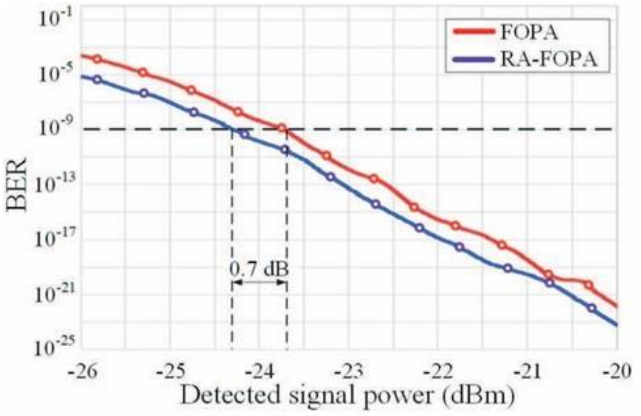

Fig. 2.4. *BER* dependence on received signal power in channel 16 in a system with RA-*FOPA* (blue line) and in a system with a single pumping *FOPA* (red line).

Figure 2.4 shows that the system with the *RA-FOPA* solution exhibited a signal that was 0.7 dB weaker at a *BER* threshold below 10–9 than the system with a standard single pumping source FOPA.

Summary of Thesis 1

- Based on the research conducted and the results obtained, it can be concluded that the amplifier configuration with a 3 W pumping light source at a wavelength of 975 nm for *WDM* applications requires a 7 m long *EYDF* (with the obtained physical parameters) and a direct pumping direction. Given the low input signal power (+20 dBm/per channel), *EYDFA* can be used to amplify up to 40 *DWDM* channels in the C-band, providing a maximum output power of +22 dBm, 19.7–28.3 dB gain and noise figure of 3.7–4.2 dB.

3. GENERAL CHARACTERISTICS AND EVALUATION OF PICOSECOND PULSE EXPANSION IN PPM COMMUNICATION SYSTEMS

The pulse position modulation (*PPM*) technique allows for a significant increase in energy efficiency compared to existing technologies [39, 40]. The *PPM* symbol (see Fig. 3.1), in which the pulse has four positions and all symbols are separated by a guard interval T_g, is intended for information processing. This figure also shows that the total time for a specific useful load interval is $M \cdot \tau = T$ – T_g, where M is the number of positions, τ is the duration of one position, and T is the duration of the symbol. The number of bits transmitted in one symbol, B, can be calculated as follows:

$$B = log_2 \times M. \quad 3.1.$$

Symbols with a higher number of positions M save energy, while a higher transmission speed is achieved by reducing the number of positions. The data transmission speed R can be calculated as follows:

$$R = \frac{B}{T}. \quad 3.2.$$

PPM as a data modulation method essentially poses seemingly simple requirements. It is necessary to ensure very short pulse generation with the possibility of changing the interval between pulses. There are many different methods for determining this. One of the most promising high-speed *PPM* techniques is direct time measurement using an event timer. The accuracy of the event timer is one of the limiting factors of this modulation method [41]. To save energy, the pulses must be as short as possible, while for detection, the pulse duration must be long enough to be recorded by the timer. The highly accurate Eventech A033-ET event timer [42, 43] can detect events with a root mean square (*RMS*) accuracy of approximately 3 ps, but the pulse must be above the timer's pulse detection threshold of at least 700 ps. Therefore, in most cases, pulse shaping, expansion, and automatic gain control must be performed before the event timer detects the pulse.

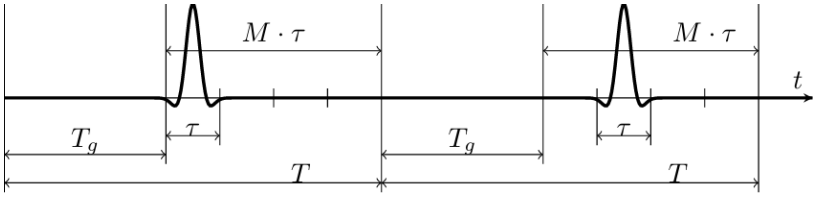

Fig. 3.1. PPM signal structure, where $M = 4$, $B = 2$, and codes are “00” and “01”.

3.1. Description of the design model of a fabricated 450 MHz low-pass filter

The design of the *LPF* model, which was fabricated and used in this experiment, is shown in Fig. 3.2. Unfortunately, both Ansys *HFSS* modeling and the experiment showed that such a self-made *LPF* filter has insufficient attenuation in the frequency band above 4 GHz, which causes significant distortion of the expanded reference pulse position modulation *512-TR-PPM* pulse shape. It should be noted that the *RF* baseband bandwidth occupied by such *PPM* signals is approximately 20 GHz.

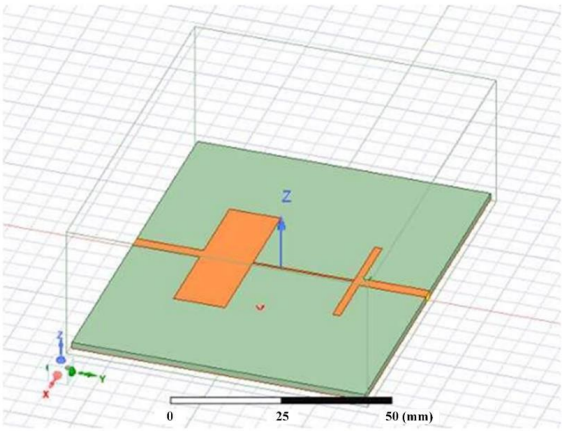

Fig. 3.2. Fabricated 450 MHz LPF design model

3.2. Evaluation of pulse expansion using various fabricated LPF filters

The experimentally constructed circuit with a pulse expansion module (*PPM*) and event timer is shown in Fig. 3.3.

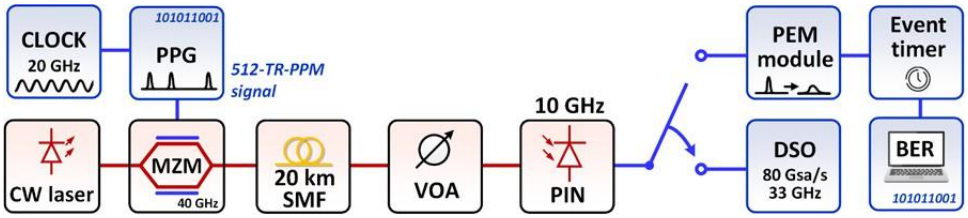

Fig. 3.3. Experimental setup for generating, transmitting and detecting a *512-TR-PPM* signal using a *DSO* or event timer with a connected computer that evaluates the *BER* of the received *PPM* signal.

The vector describing the *512-TR-PPM* waveform was saved in a special pulse pattern generator (*PPG*) file format and loaded into its memory so that it can be electrically generated

on demand. The same *PRBS* sequence is later used for *BER* estimation in the receiver. The electrical 512-TR-PPM signal was generated at the single-channel output of a *PPG* generator (*PPG*, 33 GHz, Anritsu MU183020A). The *PPG* output voltage swing is 3.5 Vpp, which is sufficient to drive the optical modulator without an additional electrical radio frequency (*RF*) amplifier. A microwave signal generator (Anritsu, 31.8 GHz, MG3693C) generates a high-purity 20 GHz sinusoidal signal and serves as the external clock source for the PPG. The 40 GHz Mach-Zehnder modulator (MZM, Photline MX-LN-40) is directly connected to the *PPG* output using a 2.92 mm to 1.85 mm connector adapter. An adjustable CW laser operating at 1552.52 nm (193.1 GHz, according to the *ITU-T DWDM* grid specification) is connected to the *MZM* input.

The optical output power is set to +7 dBm for optical (*B2B*) transmission and +9 dBm for a 20 km single-mode fiber (*SMF*) transmission configuration. After optical modulation, the signal was transmitted over 20 km of ITU-T G.652 SMF fiber. The *SMF* output is connected to a linear variable optical attenuator (VOA, Keysight FVA-3150) with 2 dB insertion loss at a wavelength of 1550 nm. The optical signal from the *VOA* output was fed to a 10 GHz *PIN* photodiode (*PIN*, 8 GHz, Amonics PR10G), where it was converted back into an electrical signal and, after passing through the PPM module, was recorded with a 33 GHz real-time digital memory oscilloscope (*DSO*, 80GSa/s, Keysight DSOZ334A) or an event timer (Eventech, A033-ET), as shown in Fig. 3.3. The RF baseband bandwidth of a *512-TR-PPM* signal with a pulse width of 50 seconds is approximately 20 GHz. In the case of optical *B2B* transmission, the pulse width of the *512-TR-PPM* signal, which was originally 50 seconds, was measured at 71 seconds. Furthermore, after 20 km of *SMF* transmission, the pulse duration is approximately 96 seconds because the *RF* bandwidth of the *PIN* receiver is limited by the chromatic dispersion of the optical fiber.

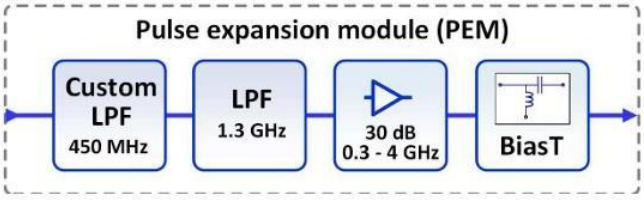

Fig. 3.4. Schematic diagram of the experimental *PEM* pulse expansion module.

An event timer was used in this experiment, for which the pulse waveform and duration are very important. The experimental *PEM* module, which was developed using a methodology already described in [68], includes the circuit shown in Fig. 3.4).

Numerical calculations in *Ansys HFSS* modeling software show that a high-order electrical *LPF* was used, whose insertion losses increase rapidly above the cutoff frequency, resulting in a wave-like filtered pulse waveform. The false ripple was also confirmed by experiments with commercial *LPFs*, manufactured with a sharp increase in insertion loss in the stopband. Calculations show that sufficient pulse width and minimal ripple in the filtered pulse waveform can be achieved using a filter with a third-order Bessel transfer function and a cutoff frequency of 450 MHz. Such a low-pass filter also ensures that the rising edge of the pulse is as steep as possible.

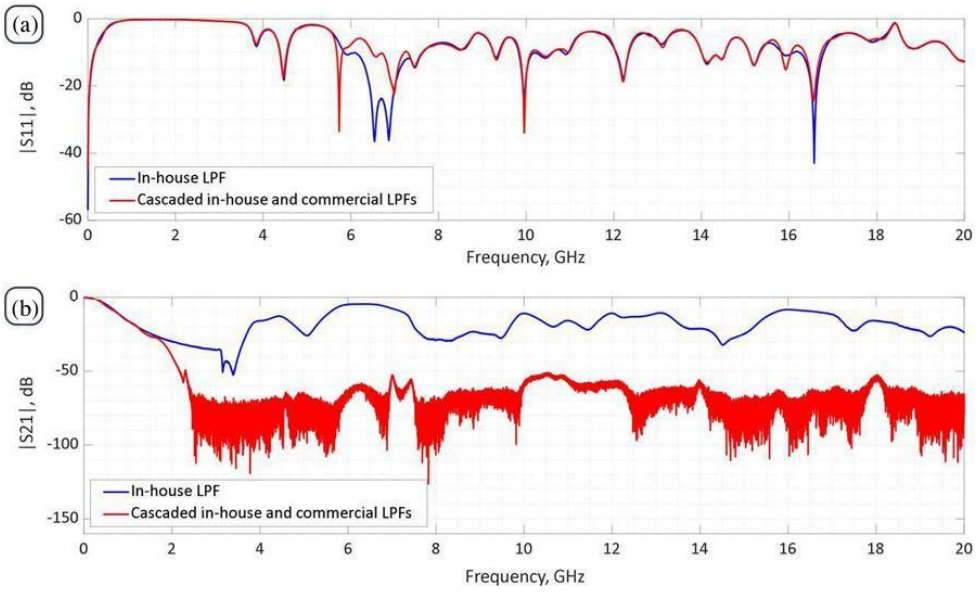

Fig. 3.5. Measured S-parameters: a) S11 curve (blue) of the *LPF* itself and (red) of the *LPF* itself and the commercial *LPF* cascade connection; b) S21 curve (blue) for the *LPF* itself and (red) for the *LPF* itself and the commercial *LPF* cascade connection.

The measured S-parameters of the fabricated LPF are shown in Fig. 3.5, where the blue curves represent the S-parameters obtained using a vector network analyzer (Rohde & Schwarz, 20 GHz, R&S ZNB20). To compensate for insufficient attenuation, a commercial *LPF* (DC-1300 MHz passband, Mini-Circuits VLFX 1300+) was connected to the self-made

cascade *LPF* filter. The measured S parameters are shown in Fig. 3.5 as red curves. The cascade LPF with a cutoff frequency of 450 MHz and a commercial filter with a cutoff frequency of 1300 MHz ensure the required pulse length increase above the 700 ps threshold (event timer requirement).

At the same time, the *PPM* retains the steep rising edge of the expanded *PPM* pulse and insignificant pulse fluctuations. After processing, by connecting a self-made cascade and commercial *LPFs*, the expanded *512-TR-PPM* signal is amplified with an RF amplifier (30 dB gain, 30–4000 MHz), and, using a bias tee (BiasT, 20 kHz 45 GHz, SHF BT45), an additional bias voltage was applied to optimize the reception of the expanded *512-TR-PPM* waveform with an event timer (Eventech, A033-ET). Using the aforementioned *PPM* module, the received *512-TR PPM* pulses were expanded to 978 ps in the receiver section, ensuring stable timer operation.

Low-order *TR-PPM* signals can be demodulated using the autocorrelation of the received signal [44]. Signals with a large number of positions *M* require more complex methods. In this study, a *512-TR-PPM* signal demodulator based on an event timer (Eventech, A033-ET) and a software framework described in [45] was used. The A033-ET is a computerized device that records time stamps (raw data) as absolute times with high accuracy (approximately 3 seconds geometric mean), and can record events at a rate of 20 M events per second. The event timer cannot detect short pulses, such as 50 ps. Therefore, a *PEM* module was created that provided 512 TR-PPM pulses with a duration of approximately 978 ps (see Fig. 4.7). A033-ET has a 50 ns dead time required for the timer to process and store data.

Summary of Thesis 2

Based on the research conducted and the results obtained, it can be concluded that 512-TR-PPM is an effective modulation mode for long-distance communications, where energy efficiency is a very important factor. The main advantage of *TR-PPM* is its stability, given the reference pulses included in each frame. This study proves that it is possible to use software to correct minor inaccuracies in signal generation, which are mainly caused by the detection method, i.e., the event timer. Using the *PPM* module in the receiver part, it is possible to extend the received *512-TR-PPM* pulses to 978 ps, ensuring stable operation of the event timer.

4. DESCRIPTION OF THE LENS FIBER APPLICATION IN INTEGRATED PHOTONIC DEVICES

This chapter demonstrates the production of spherical lens fibers (*SLF*) using commercially available arc fusion splicing (Fujikura-100P+), which is common equipment used in the field of optical fiber communications and photonics. The main objective of the study is to determine how easily important lens fiber parameters, such as working distance and diameter size, can be manipulated using this manufacturing method [46–51]. This assessment includes manufacturing simplicity, consistency of manufactured samples, and the number of iterations required to refine the lens parameters necessary for a specific application. The manufactured samples are compared with commercial-grade lens fiber products, which are used as a basis for comparison.

4.1. Description of the lens fiber structure and manufacturing process

The most common and effective method of manufacturing optical lenses involves the use of arc discharge welding equipment. In this case, an electric arc created by two electrodes fuses the fibers, thereby connecting, narrowing, and forming micro-lenses. However, the main disadvantages of this method are uneven fiber heating and long production times (up to several minutes), depending on the lens diameter. This increases the risk of geometric distortion, mainly due to the effect of gravity, but also due to external factors such as vibrations that occur during the process. Another limiting factor is that electric arc fusion splicing causes uneven heating of the outer surface of the optical fiber. This limits the ability to precisely form lens structures. All this can lead to structural asymmetry, especially if the fibers are not perfectly aligned during arc discharge [52, 53].

The first step in the lens fiber manufacturing process is to measure the total loss of the test equipment. Each piece of fiber and connector used here has a characteristic loss factor. Therefore, an uncut fiber connection cable is used at the beginning to determine the base reference value. The connector fiber cable was cut in half, considering the system power loss. This gives us the free space loss figure, where the two ends of the *SMF* (ITU-T G.652) fiber are tightly connected relative to their core profiles. Ideally, this adds only an additional 0.5 to 1 dB loss to the reference measurement figure and, in terms of transmission power, should be equal to or greater than the best lens fiber samples. Two Thorlabs motorized positioning stages are used to align both fiber ends and create a lens fiber standard fiber connection.

These stages are covered by two fiber clamps that hold the samples firmly in place to ensure optimal measurement stability. The clamps can be moved in the X, Y, and Z directions using stepper motors for broader alignment or piezo motors for precise adjustment and finding the absolute best connection position. Two microscopes are positioned directly above and to the side to ensure optimal visibility and monitoring. The end of the transmission fiber (the direct laser output element) was inserted into one end of the fusion splicer. A Fujikura *FSM-100P+* fusion splicer was used during the experiments.

4.2. Evaluation of insertion loss at a wavelength of 1550 nm

Unlike in the previously described research [54], it was decided to avoid additional core-free fiber splicing. This was justified by the fact that small lens fiber diameters would remain intact, thus avoiding additional dispersion and eliminating the fusion point between the two types of fibers. The experimental setup used is shown in Fig. 4.1.

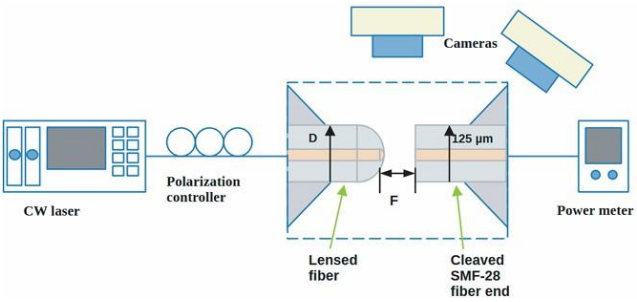

Fig. 4.1. Experimental setup for testing transmission between the separated SMF fiber and the prepared lens fiber. Here, *CW* denotes a continuous wavelength laser source.

From the experimental results shown in Fig. 4.2, it can be concluded that connection losses are not linearly related to the diameter of the lens fiber. The trend starts with a negative slope, and the best results were actually observed at a lens size of approximately 129 µm. This is followed by a gradual and rapid increase, which eventually levels off. These results could be explained as follows: in the case of very small sizes, the end of the fiber cannot form a sufficiently good lens shape because there may not be enough material around it to form the shape. It could also be that the arc discharge power is insufficient and cannot be increased because it simply creates a larger lens. As the size increases, the cause of the lens fiber problem could be related to uneven melting of the fiber core and subsequent deformation.

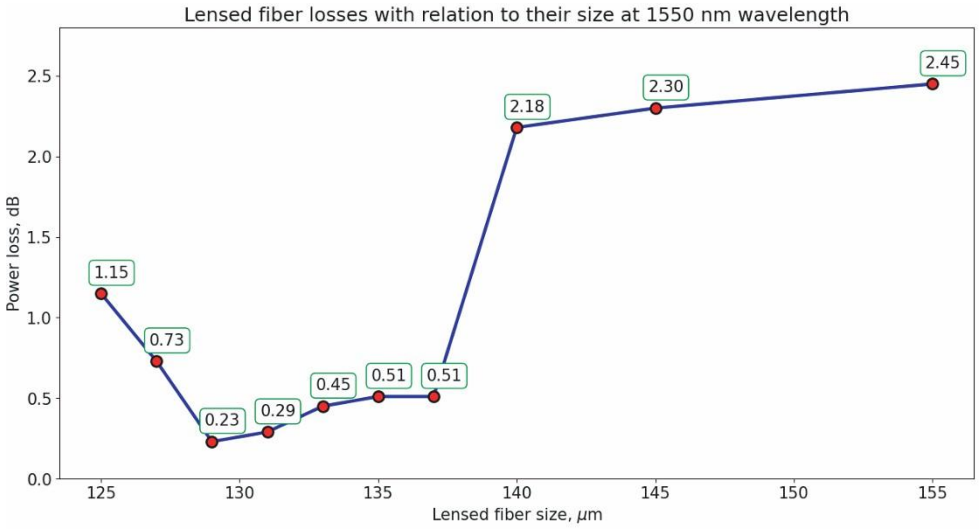

Fig. 4.2. Connection losses for a specific lens size at a wavelength of 1550 nm.

From the results shown in Fig. 4.2, it can be concluded that connection losses are not linearly related to the diameter of the lens fiber. The trend starts with a negative slope, and the best results were actually observed at a lens size of approximately 129 µm. This is followed by a gradual and rapid increase, which eventually levels off. These results could be explained as follows: in the case of very small sizes, the end of the fiber cannot form a sufficiently good lens shape because there may not be enough material around it to form the shape. It could also be that the arc discharge power is insufficient and cannot be increased because it simply creates a larger lens. As the size increases, the cause of the lens fiber problem could be related to uneven melting of the fiber core and subsequent deformation.

The principle of laboratory-made lens fibers is based on the fact that light is partially scattered from the end of the core and then focused by the welding equipment due to the shape of the lens. However, if the lens size varies too much, the results become significantly worse. This threshold occurs at a lens size of approximately 140 µm, where Fig. 4.3 (microscope image) shows the distorted core development phases.

It should be noted that during the testing phase, lens sizes ranging from 125 µm to 137 µm in diameter were tested more extensively than those ranging from 140 µm –155 µm in diameter. The smaller diameter gave better results [55]. Therefore, the gradual increase at the end of the graph may be random in nature and, for the reasons mentioned above, should be steeper.

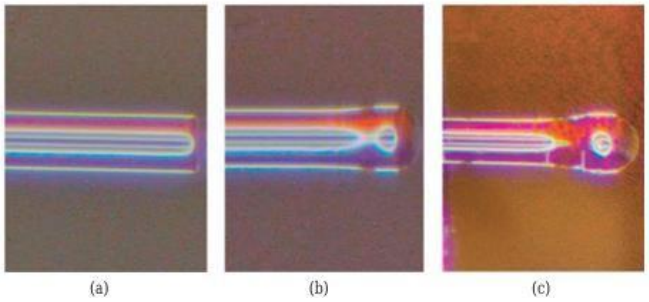

Fig. 4.3. Gradual increase in lens fiber diameter and subsequent core deformation: (a) split fiber end with a diameter of 125 µm (connected to a low power source that does not form a lens shape only in the fiber core); (b) manufactured lens fiber with a diameter of 131 µm; (c) manufactured lens fiber with a diameter of 155 µm.

In the final part of the experiment, the loss change indicators in the lens fiber system were studied and evaluated when subjected to wavelength fluctuations. This is a potentially important factor in determining their usefulness in testing optical microchips. Optical microchip waveguides tend to have different responses to different optical frequencies, and this information is essential for the operation of existing designs as well as future prototypes. This means that a certain degree of consistency in the response of the lens fiber is required in order to eliminate this factor in the testing of optical lens fibers. Figure 4.4 shows that even the best samples (127–135 µm) tend to have more or less constant responses to changes in laser frequency. Slight deviations may occur due to minor changes in the fiber condition and fluctuations in room and fiber temperature.

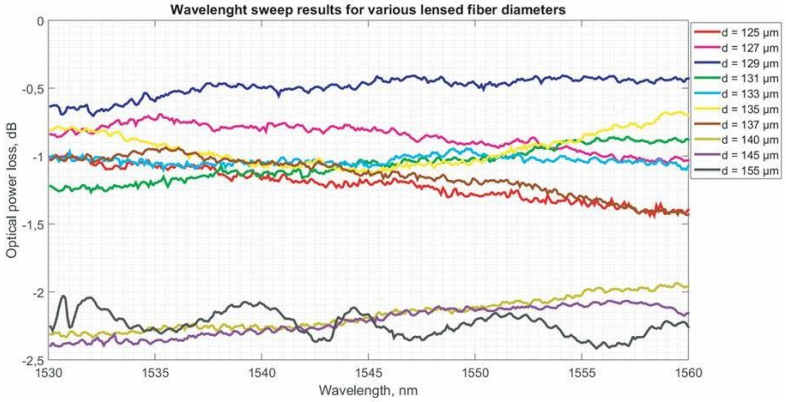

Fig. 4.4. Response of different lens sizes to changes in laser frequency (laser sweeping in the optical C-band).

Theoretically, even large-sized fiber lenses exhibit only a 0.5 dB deviation in optical power, which is within the normally acceptable error range. However, the trend line is more or less linear, which does not indicate random changes in system parameters. In addition, modern optical devices are much more accurate and sensitive to changes in laser power. Therefore, this trend cannot be ignored and can be considered a reason not to include large lens sizes in the measurements.

Summary of Thesis 3

Laboratory experiments have shown that the fabricated and demonstrated lens fibers can fulfill this role while maintaining acceptable performance indicators. Assuming that the manufacturing process has been developed, the production time for these samples is up to half an hour. The frequency shift response is consistent and reliable for the best lens fibers, which may be the most important factor, apart from the absolute loss figures for a single specific wavelength.

Therefore, it can be concluded that the fabrication of a lensed fiber from a section of standard SMF-28 optical fiber provides satisfactory performance for the intended application. Such small-diameter lensed fibers exhibit low insertion losses, efficient focusing characteristics, and high sensitivity to laser frequency variations, making them a suitable solution for the characterization and testing of optical devices where extremely high measurement precision is not required.

CONCLUSIONS

1. *EYDFA* with cladding pumping operation is characterized using a developed simulation system based on measurement data. By analyzing the amplifier gain, noise figure, and power loss, its suitability for operation in metro access optical transport networks, where *DWDM* communication system technologies are commonly used, was observed. First, double- clad Er3+/Yb3+ co-doped fiber, which was used as the gain medium for the amplifier prototype, was experimentally characterized in order to develop and analyze the experimental *EYDF* prototype. Next, various *EYDFA* configurations were tested under different operating conditions (including different lengths of alloyed fibers, pumping signal propagation directions, signal input power, etc.) to discover the parameter settings that provide the best amplification characteristics, i.e., high, uniform amplification and low noise factor. Based on the research conducted and the results obtained, it was found that for an amplifier configuration with a 3 W pump light source at a wavelength of 975 nm for *WDM* applications, a 7 m long *EYDF* (with the obtained physical parameters) and co-propagation are required. Given the low input signal power (–20 dBm/per channel), *EYDFA* can be used to amplify up to 40 *DWDM* channels in the C-band, providing a maximum output power of +22 dBm, 19.7–28.3 dB gain, 3.7–4.2 dB noise figure, and power reduction (relative to a system without amplification) below 0.1 dB at a *BER* level of 10^{-9}**.**

2. A prototype of the *EYDFA* amplifier with cladding pumping was developed using numerical simulations and an experimentally created model. An *EYDFA* configuration (total fiber length, pumping power, input signal power) suitable for signal amplification in a multi-channel optical fiber transmission system with dense wavelength division in the C-band was determined. *EYDFA* was used as the active amplification medium in commercial double-clad *EYDF* fibers. Therefore, the characteristics of *EYDF* (specifically, Er3+ and Yb3+ absorption and emission cross sections and overlap coefficients) were first determined experimentally. This data was then entered into a simulation model to determine some initial *EYDFA* settings, such as the EYDFA length and pumping power required to provide the desired amplification, before moving on to laboratory parameter configurations. Finally, the developed prototype was used to study the absolute gain and gain uniformity of the *EYDFA* under various conditions using a 48-channel *DWDM* system with −20 dBm/ch. input power. The results obtained show that the *EYDFA* amplifier prototype, consisting of a 5 m *EYDF* fiber length, where the optical pumping light source used was a multimode light-emitting diode with 2 W output power, provides practical amplification in the wavelength range of 1534–1565 nm. In this wavelength

range, the *EYDFA* provides > 21 dB of amplification per channel with a 12 dB gain coefficient, amplifying 48 channels with a 100 GHz spacing between channels.

3. Based on the research experimental results, it can be concluded that the BER threshold of 1×10^{-9} was achieved at a pumping power of 80 mW for co-propagating pumping ($\lambda = 980$ nm) and at 130 mW pumping power for counter-propagating pumping direction ($\lambda = 1480$ nm) for a 10 Gbit/s *NRZ* modulated received worst-case signal operated at λ.

4. Comparing the OSNR values of all channels after amplification, it was found that the *OSNR* in the *RA-FOPA* system is on average 0.8 dB higher than in the single-pump *FOPA* system. This result can be explained as follows. The *FWM* process used by *FOPA* for signal amplification is highly dependent on the phase mismatch between the interacting spectral components (pump and signal). On the one hand, the signal and parametric amplifier pumping jointly propagate in the *HNLF*, so the greater the accumulated phase mismatch, the lower the *FWM* efficiency. On the other hand, the efficiency of FWM increases with the power of the interacting spectral components. This applies not only to pump-signal interaction (amplification), but also to channel-channel interaction (*CC-FWM*). Therefore, if the parametric amplifier pumping has an additional power source throughout the amplification process, the main part of the amplification is generated further in the *HNLF*, where the efficiency of *CC-FWM* and parametric amplification is lower than at the beginning of the amplification environment. The difference in interchannel overlap caused by *CC-FWM* resulted in a 0.7 dB power reduction in the system with a standard single-pump source FOPA compared to the system with an *RA-FOPA* solution, ensuring the required received signal $BER \geq 1 \times 10^{-9}$ threshold.

5. Based on the research conducted and the results obtained, it can be concluded that 512-*TR-PPM* is an effective modulation mode for long-distance communications, where energy efficiency is a very important factor. The main advantage of *TR-PPM* is its stability, given the reference pulses included in each frame. The results obtained prove that it is possible to use software to correct minor inaccuracies in signal generation, which are mainly caused by the detection method, i.e., the event timer. The use of an event timer for *PPM* signal detection offers many advantages, such as the ability to analyze raw data (timestamps) and apply digital signal processing for correction in the receiver. By using a *PPM* module in the receiver section, it was possible to extend the received *512-TR-PPM* pulses to 978 ps, ensuring stable operation of the event timer.

6. The results show that the position width significantly affects the *BER* of the *PPM* signal. The main obstacle to achieving low *BER* at narrower time intervals is jitter, which

allows higher data transfer rates at the event timer input. An inaccurate *PPM* modulator can introduce jitter in the form of waves using *PPG*, which is not a significant cause of jitter. A much greater impact is likely to be caused by the analog front end of the *PPM* receiver, which consists of a *PEM* containing an *RF* amplifier and deviation elements.

7. Finally, lensed fiber samples were made from core-less fiber using a commercial fusion arc splicer. The light beam diverges more when connecting a longer piece of core-less fiber to *SMF*. Combined with the focusing properties of the manufactured lens, this provides a tighter focus, resulting in reduced connection losses. Lens fibers with high connection losses can be used in various applications, where precise light focus and control are required. Despite higher connection losses, these applications include biomedical imaging or *FBG* sensors, where the high connection losses of lens fibers can help reduce unwanted reflections and improve the signal-to-noise ratio. Overall, lens fibers with high coupling losses can be useful in microchip applications that require precise light coupling control, high signal-to-noise ratio, and low signal reflections.

LIST OF REFERENCES

1. Lipatov, D. S.; Lobanov, A. S.; Guryanov, A. N.; Umnikov, A. A.; Abramov, A. N.; Khudyakov, M. M.; Likhachev, M. E.; Morozov, O. G. Fabrication and Characterization of Er/Yb Co-Doped Fluorophosphosilicate Glass Core Optical Fibers. *Fibers* **2021**, *9*, 15. doi: 10.3390/fib9030015.
2. "Cisco visual networking index — Forecast and methodology 2017–2022, cisco systems", White Paper, No. 1, 2018.
3. Routray S. K., A. Javali, R. Nyamangoudar, and L. Sharma, "Latching on to Keck's Law: Maintaining the high speed trends in optical communication", 4th Int. Conf. Advanced Computing and Communication Systems (ICACCS 2017), 1–5, Coimbatore, 2017, doi: 10.1109/ICACCS.2017.8014637.
4. He L, Chen Y, Yin X, Gu Z, Liu S, Li W, Xing Y, Chu Y, Dai N, Li J. "High-efficiency cladding-pumped Er/Yb co-doped alumino-phosphosilicate fiber for an extended L-band amplification". Opt Lett. 2024 Jan 1; 49(1):61–64. doi: 10.1364/OL.509954. PMID: 38134152.
5. Putrina J., Olonkins S., and Bobrovs V. "Investigation of in-line EDFA performance dependence on channel spacing in WDM transmission systems" 2016 Advances in Wireless and Optical Communications (RTUWO), 17–21, Riga, 2016, doi: 10.1109/RTUWO.2016.7821848.
6. Lipatov D., Egorova O., Rybaltovsky A., Abramov A.; Lobanov A.; Umnikov A., Yashkov, M.; Semjonov, S. "Highly Er/Yb-Co-Doped Photosensitive Core Fiber for the Development of Single-Frequency Telecom Lasers". *Photonics* 2023, *10*, 796. doi: 10.3390/photonics10070796.
7. Yu W., Yan P., Xiao Q., Qi T., Li D., Gong M. "Power scalability of a continuous-wave high-power Er-Yb co-doped fiber amplifier pumped by Yb-doped fiber lasers". Appl Opt. 2021 Mar 1; 60(7):2046–2055. doi: 10.1364/AO.416515. PMID: 33690297.
8. Féron P., Rasoloniaina A., Huet V., Le Cren E., Trebaol S., Nunzi Conti G., Serier-Brault H., Mortier M., Dumeige Y. "High gain selective amplification in whispering gallery mode resonators: analysis by cavity ring down method", Proceedings Volume 8600, Laser Resonators, Microresonators, and Beam Control XV; 86000G (2013) doi: 10.1117/12.2002821.
9. Tough Euan John, "Integrated Optical Frequency Comb Generation For Photonic Terahertz Synthesis", 2 February, 2024.

10. Zhang Hao., Chang Bing., Li Zhaoyu., Liang Yu-Pei., Qin Chen-Ye., Wang Chun., Xia Han-Ding, Tan Teng., Yao Bai-Cheng. "Coherent optical frequency combs: From principles to applications", Journal of Electronic Science and Technology, Volume 20, Issue 2, 2022. doi: 10.1016/j.jnlest.2022.100157.

11. Shu Haowen., Shen Bitao., Chang Huajin., Han Junhao., Xiao Jiong., Wang Xingjun. "Microcomb technology: from principles to applications", Photon. Insights 3, R09 (2024). doi: 10.3788/PI.2024.R09.

12. Gao D., Li T., Xie Z., He Y., Han X., Jia S., Wang W., and Xie X. (2022) "Performance evaluation of the high-speed deep-space optical communication system assisted by preamplified thresholded pulse-position modulation". Front. Phys. 10:987994. doi: 10.3389/fphy.2022.987994.

13. Hyun Y., Park H., Han S. "Enhanced Pulse-Position Optical Modulation based on Optical Delay Interferometer for Satellite Optical Communication" in 2024 Conference on Lasers and Electro-Optics Pacific Rim (CLEO-PR), Technical Digest Series (Optica Publishing Group, 2024), paper Th1K_5.

14. Cisco Systems Inc. DWDM Networking Primer. ONS 15454 MSTP. White paper. – October 2003. – 87 p.

15. Gumaste A., Antony T. "DWDM Network Designs and Engineering Solutions". – USA: Cisco Press, 2002. – 368 p. ISBN: 978-1-58705-074-9.

16. Zyskind, J., Srivastava, A. Optically. Amplified WDM Networks. First edition. – USA: Academic Press, 2011. – 502 p. ISBN: 978-0-12-084590-3.

17. Hecht J. Understanding Fiber Optics. Fourth Edition. – NJ: Prentice Hall, 2002. – 780 p. ISBN: 978-0-1302-7828-9.

18. Ramaswami R., Sivarajan K., Sasaki G. Optical Networks: A Practical Perspective. Third Edition. – USA: Morgan Kaufmann, 2009. – 928 p. ISBN: 978-1-5586-0-4452.

19. Yoshikane N., Tsuritani T. "Recent progress in space-division multiplexing optical network technology". In Proceedings of the 2020 International Conference on Optical Network Design and Modeling (ONDM), Barcelona, Spain, 18–21 May 2020; pp. 1–4. doi: 10.23919/ONDM48393.2020.9133031.

20. Takeshima K., Tsuritani T., Igarashi K., Morita I., Tsuchida Y., Maeda K., Saito T., Watanabe K., Sasa T., Imamura K., et al. "WDM/SDM transmission of 76 128-Gbit/s Nyquist-pulse-shaped DP-QPSK Signals over 4,200 km using cladding pumped 7-Core

EDFA". *2015 Opto-Electronics* and Communications Conference (OECC), Shanghai, China, 2015, pp. 1–3, doi: 10.1109/OECC.2015.7340111.

21. Dutton H. J. R. Understanding Optical Communications. – NJ: Prentice Hall, 1998. – 760 p. ISBN: 978-0-1302-0-1416.

22. Chomycz B. Planning Fiber Optics Networks. – USA: McGraw Hill Professional, 2009. – 320 p. ISBN: 978-0-07-164269-9.

23. Matsumoto, K., Seno, K., Mizuno T., Yanagimachi S., Gaborv E. L. T. D., Mivamoto Y. "Experimental demonstration of a SDM node with low power consumption MC-EDFA and SPOC-based WSS arrays". In Proceedings of the 2019 24th OptoElectronics and Communications Conference (OECC) and 2019 International Conference on Photonics in Switching and Computing (PSC), Fukuoka, Japan, 7–11 July 2019; pp. 1–3. doi: 10.23919/PS.2019.8817883.

24. Thyagarajan K., Ghatak A. Fiber Optic Essentials. NJ: John Wiley & Sons, 2007. – 259 p. ISBN: 978-0-470-09742-7.

25. Thouras J., Pincemin E., Amar D., Gravey P., Morvan M., Moulinard, M.-L. "Introduction of 12 cores optical amplifiers in optical transport network" Performance study and economic impact. In Proceedings of the 2018 20th International Conference on Transparent Optical Networks (ICTON), Bucharest, Romania, 1–5 July 2018; pp. 1–4. doi: 10.1109/ICTON.2018.8473674.

26. Jain S., Castro C., Jung, Y., Hayes, J., Sandoghchi, R., Mizuno T., Sasaki Y., Amma Y., Miyamoto Y., Bohn M., et al. "32-core erbium/ytterbium-doped multicore fiber amplifier for next generation space-division multiplexed transmission system". Opt. Express 2017, 25, 32887–32896, doi:10.5258/SOTON/D0246.

27. Torounidis T., Andrekson P. A., Olsson B.-E., "Fiber-optical parametric amplifier with 70-dB gain". IEEE Photonics Technology Letters, Vol. 18, No. 10, 11941196, May 2006, doi: 10.1109/LPT.2006.874714.

28. Jamshidifar, M., A. Vedadi, and M. E. Marhic, Continuous-wave one pump fiber optical parametric amplifier with 270 nm gain bandwidth, Proc. ECOC, paper 1.1.4, Sep. 12, 2009, doi: 10.1109/LPT.2006.874714.

29. Jamshidifar M., Vedadi A., Marhic M. E. in: Tech. Digest of 37th ECOC 2009, paper Mo1.1.4, Vienna, 2009.

30. Karasek M., Honzatko P., Vojtech J., Radil J., "Multi-wavelength conversion at 10Gb/s and 40Gb/s based on 2 pumps FOPA". 2011 13th International Conference on Transparent Optical Networks, 14, Stockholm, 2011, doi: 10.1109/ICTON.2011.5970951.

31. Gnauck A. H., Jopson R. M., "Dispersion compensation for optical fiber systems, Optical Fiber Telecommunications". IIIA, 162195, I. P. Kaminow and T. L. Koch, Eds., Academic, San Diego, CA, 1997, doi: 10.1109/35.387557.

32. Wang J., Ji Hua., Hu Hao., Mulvad H-C., Galili M., Palushani E., Jeppesen P., Yu J., Oxenlowe L.K. "All-optical 2R regeneration of a 160-Gbit/s RZOOK serial data signal using a FOPA" IEEE Photonics Conference 2012, 108-109, Burlingame, CA, 2012, doi: 10.1109/IPCon.2012.6358512.

33. Wang Ju., Yu Jinlong., Luo Jun., Wang W., Han B., Wu Bo., Yang E. "40-Gb/s 2-channel all-optical 3R regeneration using data-pumped fiber para metric amplification based on HNLF". Asia Communications and Photonics Conference and Exhibition, 86–87, Shanghai, 2010, doi: 10.1109/ACP.2010.5682823.

34. Marhic M. E. "Fiber Optical Parametric Amplifiers, Oscillators and Related Devices" 366, Cambridge University Press, University of Wales, Swansea, 2007, doi: 10.1017/CBO9780511600265.

35. Agrawal Govind P. – Nonlinear Fiber Optics, 5th ed., Academic Press, 2013.

36. Várallyay Z., Szabó A., Rosales A., Gonzales E., Tobioka H., Headley C. "Accurate modeling of cladding pumped, star-shaped, Yb-doped fiber amplifiers". Opt. Fiber Technol. 2015, 21, 180–186, doi: 10.1016/j.yofte.2014.11.003.

37. Supe A., Olonkins S., Udalcovs A., Senkans U., Murnieks R., Gegere L., Prigunovs D., Grube J., Elsts E., Spolitis S.; Ozolins, O., Bobrovs V. "Cladding-Pumped Erbium/Ytterbium Co-Doped Fiber Amplifier for C-Band Operation in Optical Networks". Appl. Sci. 2021, 11, 1702, doi: 10.3390/app11041702.

38. Bai X., Wang M., Yang Y., Liu Z., Jia W. "Experimental and Theoretical Analysis on Pump Spectral Propriety of Single Frequency Erbium-Ytterbium Co-Doped Fiber Amplifier". J. Phys. Commun. 2021, 5, 015005, doi: 10.1088/2399-6528/abd8ec.

39. Zhou Z., Liang B., Cao Y., Zhang M. (2022, January). MPPM Spectrum Analysis Based on PPM. In 2022 14th International Conference on Computer Research and Development (ICCRD) (pp. 356–362). IEEE, doi: 10.1109/ICCRD54409.2022.9730597.

40. Tang W., Wang S., Xu Y., Yu, Z. (2022). "The research process, application, and the future development of pulse-position modulation". Journal of Physics: Conference Series, 2384 (1), 012026. doi: 10.1088/1742-6596/2384/1/012026.

41. Migla, S.; Rubuls, K.; Tihomorskis, N.; Salgals, T.; Ozolins, O.; Bobrovs, V.; Spolitis, S.; Aboltins, A. Ultra-Wideband Analog Radio-over-Fiber Communication System

Employing Pulse Position Modulation. Appl. Sci. 2025, 15, 4222. doi: 10.3390/app15084222.

42. Eventech Ltd, Event Timer A033 ET / usb. [Online]. Available: http://eventechsite.com/en/products/event-timer-a033-et/.

43. Migla S., Selis O., Sics P. E., Pudzs M., Zeltins M., Aboltins A. "A Design of UWB Communication Testbed with Event Timer-based PPM Demodulator", *2022* IEEE *2nd* Ukrainian Microwave Week (UkrMW), Ukraine, 2022, pp. 691–694, doi: 10.1109/UkrMW58013.2022.10037100.

44. Munirathinam R., Aboltins A., Pikulins D., Grizans J. "Chaotic non-coherent pulse position modulation based ultra-wideband communication system". 2021 IEEE Microwave Theory and Techniques in Wireless Communications (MTTW), 52 57, 2021, doi: 10.1109/MTTW53539.2021.9607075.

45. Migla S., Selis. O., Sics P. E., Pudzs M., Zeltins M., Aboltins A. "A Design of UWB Communication Testbed with Event Timer-based PPM Demodulator", *2022 IEEE* 2nd Ukrainian Microwave Week (UkrMW), Ukraine, 2022, pp. 691–694, doi: 10.1109/UkrMW58013.2022.10037100.

46. Piccirillo F., Giaquinto M., Ricciardi A., and Cusano A. "(INVITED) Miniaturized lenses integrated on optical fibers: Towards a new milestone along the lab-on-fiber technology roadmap" Results Opt., 2021, vol. 6, p. 100203. doi: 10.1016/j.rio.2021.100203.

47. Ghenuche, R., Rigneault, H., Wenger J. "Hollow-core photonic crystal fiber probe for remote fluorescence sensing with single molecule sensitivity" J. Opt. Express, 2012, vol. 20, no. 27, p. 28379. doi: 10.1364/OE.20.028379.

48. Allen K. W., Kosolapov A. F., Kolyadin A. N., Pryamikov A. D., Mojaverian N., Limberopoulos N. I., Astratov V. N. "Photonic jets produced by microspheres integrated with hollow-core fibers for ultraprecise laser surgery" Proc. 15th Int. Conference on Transparent Optical Networks (ICTON), Cartagena, 2013, p. 1. doi: 10.1109/ICTON.2013.6602908.

49. Zelgowski, J., Abdurrochman, A., Mermet, F., Pfeiffer, P., Fontaine, J., and Lecler, S., "Photonic jet subwavelength etching using a shaped optical fiber tip". Opt. Lett., 2016, vol. 41, no. 9, p. 2073. doi: 10.1364/OL.41.002073.

50. Bouaziz, D., Chabrol, G., Guessoum, A., Demagh, N.E., and Lecler, S., Photonics, 2021, vol. 8, no. 9, p. 373. doi: 10.3390/photonics8090373.

51. Xiong, Y. and Xu, F. "Multifunctional integration on optical fiber tips". Adv. Photonics, 2020, vol. 2, no. 6, p. 064001. doi: 10.1117/1.AP.2.6.064001.

52. Guzowski B., Lakomski M., Cywinski M. “Proximity sensors based on ball-lensed optical fibers,” IOP Conf. Ser.: Mater. Sci. Eng., vol. 104, p. 012031, Jan. 2016, doi: 10.1088/1757-899X/104/1/012031.

53. Fan K.-C., Hsu H.-Y., Hung P.-Y., Wang W. “Experimental study of fabricating a microball tip on an optical fibre”, J. Opt. A: Pure Appl. Opt., vol. 8, no. 9, pp. 782–787, Sep. 2006, doi: 10.1088/1464- 4258/8/9/012.

54. Sedulis, A., et al., “Fabrication of lensed fibers with arc fusion splicer for telecommunication applications”, 2023 Photonics & Electromagnetics Research Symposium (PIERS), 1066–1070, Prague, Czech Republic, Jul. 03–06, 2023, doi: 10.1109/PIERS59004.2023.10221315.

55. Ryu S-Y., Choi H-Y., Na J., Choi W-J., Lee B-H. “All-fiber probe for optical coherence tomography”. Proc. SPIE 6847, Coherence Domain Optical Methods and Optical Coherence Tomography in Biomedicine XII, 68472L (18 February 2008), doi: 10.1117/12.766316.

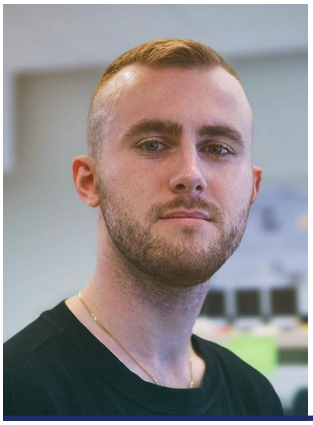

Dmitrijs Prigunovs obtained a Bachelor's degree in Electrical Engineering (2019) and an Academic Master's degree in Telecommunications Engineering (2021) from Riga Technical University (RTU). Since 2019, he has worked at RTU, initially as a scientific assistant and currently as a researcher and lecturer at the Institute of Photonics, Electronics and Electronic Communications.

His research activities focus on fibre-optic communication systems, optical amplifiers, and WDM technologies. He has participated in research projects funded by the European Union and RTU, and is a co-author of several internationally indexed scientific publications.

In addition to his research work, D. Prigunovs is actively involved in academic activities, teaching courses in Fibre-Optic Transmission Systems and the Physics of Optical Information Processing, as well as supervising bachelor's and master's theses.